Communauté
UNIVERSITÉ Grenoble Alpes

THÈSE

Pour obtenir le grade de

DOCTEUR DE la Communauté UNIVERSITÉ GRENOBLE ALPES

Spécialité : **Biologie cellulaire**

Arrêté ministériel : 7 Août 2006

Présentée par

Nils Giordano

Thèse dirigée par **Johannes Geiselmann**
et codirigée par **Hidde de Jong**

préparée au sein **Laboratoire Interdisciplinaire de Physique**
et de **Ecole doctorale Chimie et Science du Vivant**

Growth control in microorganisms : theoretical and experimental study by mean of self-replicator models

Thèse soutenue publiquement le ,
devant le jury composé de :

...Civilité, Prénom-et-Nom...
...titre-et-affiliation..., Président
M, Matthew Scott
Associate Professor, Department of Applied Mathematics, University of Waterloo, Rapporteur
...Civilité, Prénom-et-Nom...
...titre-et-affiliation..., Rapporteur
M, Matthieu Jules
Chargé de recherche, Inra, Grignon, Examinateur
M, Olivier Bernard
Chargé de recherche, Inria, Nice – Sophia-Antipolis, Examinateur
Mme, Irina Mihalcescu
Maître de conférence, Université Grenoble Alpes, LIPhy, Examinatrice
M, Johannes Geiselmann
Professeur, Université Grenoble Alpes, LIPhy, Directeur de thèse
M, Hidde de Jong
Directeur de recherche, Inria, Grenoble – Rhône-Alpes, Co-Directeur de thèse
Jean-Luc Gouzé
Directeur de recherche, Inria, Nice – Sophia-Antipolis, Invité

(dédicace ici)

Acknowledgements

(remerciements ici)

Abstract

Nam dui ligula, fringilla a, euismod sodales, sollicitudin vel, wisi. Morbi auctor lorem non justo. Nam lacus libero, pretium at, lobortis vitae, ultricies et, tellus. Donec aliquet, tortor sed accumsan bibendum, erat ligula aliquet magna, vitae ornare odio metus a mi. Morbi ac orci et nisl hendrerit mollis. Suspendisse ut massa. Cras nec ante. Pellentesque a nulla. Cum sociis natoque penatibus et magnis dis parturient montes, nascetur ridiculus mus. Aliquam tincidunt urna. Nulla ullamcorper vestibulum turpis. Pellentesque cursus luctus mauris.

Résumé

Nam dui ligula, fringilla a, euismod sodales, sollicitudin vel, wisi. Morbi auctor lorem non justo. Nam lacus libero, pretium at, lobortis vitae, ultricies et, tellus. Donec aliquet, tortor sed accumsan bibendum, erat ligula aliquet magna, vitae ornare odio metus a mi. Morbi ac orci et nisl hendrerit mollis. Suspendisse ut massa. Cras nec ante. Pellentesque a nulla. Cum sociis natoque penatibus et magnis dis parturient montes, nascetur ridiculus mus. Aliquam tincidunt urna. Nulla ullamcorper vestibulum turpis. Pellentesque cursus luctus mauris.

Contents

Chapter 1

Introduction

There's an infinity of things that have never been done before, and most of those things are not worth doing. – Jeremy Fox, *Dynamic Ecology*, 2016

Summary

In this section...

Résumé

Dans cette section...

1.1 Context and motivations

Microorganisms exhibits the most fundamental features of life. *They are open systems that take energy from the environment around them, and use it to maintain and reproduce their structures. They live literally everywhere, have the same metabolism, etc... They represent a perfect model organism for fundamental questions.*

They also managed to become the thoughest of all the living systems. *Their diversity allow them to colonize every biotope, but remarkably, a single species can live in broad conditions, growing on different carbon sources or resist to really harmful environments (even space!).*

Their capacity to survive and exploit strong environmental fluctuations lay on another ubiquitous process of life as we know it: self-catalysis and gene expression. *Short explanation on DNA, RNA, Protein and the regulations*

behind, that can be seen as loading "programs" depending on the environment the organism as to cope with.

Such a mechanism can be seen as a resource allocation problem. *Because they can build everything from a single carbon source. But they have a limited protein production capacity, so choice have to be made for what need to be produced, natural selection selecting for the best strategies.*

General growth laws have been identified. *The study of resource allocation led to fundamental laws like ribosome allocation or overflow metabolism, processes that can only be understood through growth rate maximization.*

Biomass production is an important fitness factor of microorganisms. *Broadly used in a variety of study*

One of the key feature that made these works possible was to study the living system in a well-defined and reproducible state: balanced-growth. *We describe balanced-growth, what it means for the dynamical system, and how you can reproduce it in a lab. We also explain why it is so convenient.*

The mechanisms identified exist to cope with environmental fluctuations in the natural habitat of microorganisms, but are being studied in constant environments. *Now we start to see the problem: there's a caveat in studying a system that is designed to respond to changes, if we focus on unchanging conditions. And we are currently unable to create such beautiful laws when taking into account dynamical conditions.*

While adopting a dynamical perspective on resource allocation is challenging, it could be fundamental to the life-treat-history of microorganisms. *It is also a problem if the system we are studying poorly encountered this state during its evolution. In other words, "maybe bacteria are confused during steady-state". Hence, there is really a strong need for a mathematical framework to study resource allocation in dynamical conditions, and to know what actually happens during these growth transitions.*

1.2 Problem statement

How do microorganisms adjust their resource allocation during environmental transitions ? *As we discussed, I tried to be as specific as possible here.*

1.3 Related work

(the work on dynamic, Van der Berg, Alon, Levy, etc... the work on steady-state has normally been described previously. Or, I don't know,

maybe I can shortly describe it in the context and extensively describe it here.)

1.4 Approach

We first tackle the problem of creating a mathematical framework for studying environmental transitions. *Building upon the work cited above, we create a simple self-replicator model that allocate resources between two sections.*

The goal is to identify what would be an ideal transition. *We all have an intuitive idea of what should be a good transition: it should be fast, robust, etc... But it is unclear how this relates to the fitness factor that shaped the regulatory mechanisms of microorganisms.*

We describe dynamical optimilaty by using optimal control theory. *Brieve explanation about optimal control theory and how it is used in economic or engineering to optimize or understant dynamical processes.*

Then, after we know what to look for, we try to actually measure how resource allocation occurs in a model organism: *Escherichia coli. We justify the use of coli and introduce the gene expression fluorescent reporter. We made a strain with fluorescent ribosomes, and studied our experimental framework in different transitions, at the population and the single cell level. We justify the use of both by the fact that population is easy for "screening", and single cell allow for a better resolution and take care of the "desynchronization" biais that could occur.*

1.5 Organisation of the dissertation

(announcing the plan of the manuscript, which actually follow exactly the approach part, without the lenghty justifications)

Chapter 2

Dynamical Allocation of Cellular Resources as an Optimal Control Problem: Novel Insights into Microbial Growth Strategies

Résumé du chapître 2 : [titre français]

dans cette section blablabla

2.1 Abstract

Microbial physiology exhibits growth laws that relate the macromolecular composition of the cell to the growth rate. Recent work has shown that these empirical regularities can be derived from coarse-grained models of resource allocation. While these studies focus on steady-state growth, such conditions are rarely found in natural habitats, where microorganisms are continually challenged by environmental fluctuations. The aim of this paper is to extend the study of microbial growth strategies to dynamical environments, using a self-replicator model. We formulate dynamical growth maximization as an optimal control problem that can be solved using Pontryagin's Maximum Principle. We compare this theoretical gold standard with different possible implementations of growth control in bacterial cells. We find that simple control strategies enabling growth-rate maximization at steady state are suboptimal for transitions from one growth regime to another, for exam-

ple when shifting bacterial cells to a medium supporting a higher growth rate. A near-optimal control strategy in dynamical conditions is shown to require information on several, rather than a single physiological variable. Interestingly, this strategy has structural analogies with the regulation of ribosomal protein synthesis by ppGpp in the enterobacterium *Escherichia coli*. It involves sensing a mismatch between precursor and ribosome concentrations, as well as the adjustment of ribosome synthesis in a switch-like manner. Our results show how the capability of regulatory systems to integrate information about several physiological variables is critical for optimizing growth in a changing environment.

2.2 Introduction

Microorganisms adapt their physiology to changes in nutrient availability in the environment. This involves changes in the expression of a large number of genes, encoding proteins with a variety of cellular functions, such as transporters for the uptake of nutrients, enzymes for the conversion of nutrients to energy and building blocks for macromolecules, the components of the transcriptional and translational machinery, and transcription factors to preferentially direct RNA polymerase to specific promoters [1, 2]. Fundamentally, the reorganization of gene expression in response to changes in environmental conditions is a resource allocation problem. It poses the question how microorganisms redistribute their protein synthesis capacity over different cellular functions when constrained by the changing environment.

The mechanisms responsible for resource allocation in microbial cells are usually assumed to have been optimized through evolution, so as to maximize the offspring of cells in their natural environment. How this general principle manifests itself on the level of cellular physiology is not straightforward though. Many studies have reasoned that growth-rate maximization provides a selective advantage to microorganisms, because it allows competitors to be outgrown when resources are scarce. Others have shown, however, that appropriate optimization criteria will depend on the structure of the environment and the ecosystem, as well as on the molecular properties of metabolic pathways [3–7]. For instance, in environments without competition for a shared resource, maximization of growth yield rather than growth rate is expected to provide a selective advantage. Although what counts as optimal is thus context-dependent, growth and evolution experiments in *Escherichia coli* have shown that in certain conditions bacterial metabolism is indeed geared towards growth-rate maximization [8–10].

For this reason, growth-rate maximization is a central hypothesis in a

number of recent theoretical studies of resource allocation using coarse-grained models of the cell [11–13]. The models deliberately reduce the molecular complexity of regulatory networks so as to focus on generic explanatory principles [14]. Along these lines, Molenaar *et al.* developed a series of simple models of the microbial cell, taking into account that growth requires the synthesis of proteins playing a role in metabolism (transporters, enzymes) and gene expression (ribosomes), in varying proportions. Allocation parameters that maximize the growth rate were shown to account, at least in a qualitative way, for the variation of the amount of ribosomal protein as a fraction of total protein in different growth media, and for the occurrence of overflow metabolism above certain growth rates [11]. Using another coarse-grained model of the cell, centered on amino acid supply (metabolism) and demand (protein synthesis), Scott *et al.* derived empirical growth laws with linear relations between the ribosomal protein fraction and the growth rate, in conditions where the nutrient supply or demand are altered [12, 13]. In their model, maximization of growth rate requires maximization of amino acid flux and is achieved for a specific, unique value of the ribosomal protein fraction. Based on a structurally similar model, Maitra and Dill related optimal resource allocation to the basic constants of the metabolic and gene expression machinery, in particular energy efficiency [15].

The assumption of growth-rate maximization may lead to correct predictions in some situations, but ignores the regulatory mechanisms achieving resource allocation and therefore cannot provide a causal explanation of cellular behavior [16]. Several studies have used coarse-grained models to understand which control strategies microorganisms employ to achieve (optimal) resource allocation [13, 17, 18]. Scott *et al.* have shown that a robust feedforward control strategy, based on the sensing of the amino acid pool size and the corresponding adjustment of the fraction of ribosomes producing ribosomal proteins, allows the ribosomal protein fraction to be maintained close to its optimal value under a variety of growth conditions [13]. The authors suggest that this control strategy involves the signalling molecule ppGpp, in agreement with conclusions drawn from a recent kinetic model of the regulatory mechanisms achieving optimal adjustment of the ribosomal protein fraction [17]. Weiße *et al.* also developed a coarse-grained model of microbial growth based on resource allocation trade-offs [18]. Without including specific regulatory interactions, the model accounts for the above-mentioned bacterial growth laws, predicts host-circuit interactions in synthetic biology, and relates gene regulation to the nutrient composition of the medium.

The above studies consider resource allocation at steady state, where all intensive variables describing the growing microbial culture, in particular the concentrations of its molecular components, are constant (see [19] for

a precise definition of steady-state growth and the closely related notions of balanced and exponential growth). This requires an environment to be stable over a long period of time. Such conditions can be achieved in the laboratory [20], but many microorganisms naturally experience frequently-changing conditions. For example, *E. coli* can cycle between two distinct habitats, the mammalian intestine and the earth's surface (water, sediment, soil) [21]. The bacteria transit through different microenvironments in the intestinal system, where they encounter different mixes of sugars [22]. They are even more challenged in the open environment outside the host, with a greatly fluctuating availability of carbon and energy sources and a large variability in temperature, osmolarity, oxygen, and microbial communities [23, 24].

This situation motivates a dynamical perspective on microbial growth and resource allocation [25–28]. However, fundamental results like the growth laws uncovered for steady-state conditions are still lacking. In particular, extending the results reviewed above to dynamical conditions raises the following questions: Are control strategies that maximize steady-state growth also optimal in dynamical environments? If this is not the case, then which alternative strategies would be optimal for such conditions? And finally, how do these strategies compare with the regulatory mechanisms that have actually evolved in microorganisms?

The aim of this study is to address the above fundamental questions in a specific dynamical growth scenario, namely a transition between two steady states following an environmental perturbation. In particular, we consider the upshift of a microbial culture from a medium supporting growth at a low rate to a medium supporting growth at a high rate [28]. We develop a coarse-grained model of the cell, inspired by the self-replicator model of Molenaar *et al.* [11], and reformulate our questions in the context of optimal control theory [29] to identify control schemes maximizing biomass production over an interval of time, the dynamical equivalent of growth-rate maximization.

We show that Pontryagin's Maximum Principle suggests that optimal resource allocation after a growth transition is achieved by a bang-bang-singular control law [29], a conjecture confirmed by direct numerical optimization. This optimal solution provides a gold standard against which possible control strategies of the cell can be compared. We consider simple strategies that drive the system to the steady state enabling growth at the maximal rate in the new medium, after the upshift. In a dynamical growth scenario, the strategy sensing the concentration of precursor metabolites emerges as the best candidate, consistent with the analysis of Scott *et al.* that feedforward activation of the rate of synthesis of ribosomal proteins, involving ppGpp-mediated sensing of the amino acid pool [30–32], is the key regulatory mechanism for growth control. It is possible, however, to

define a strategy approaching the theoretical optimum even more closely by exploiting information on both the precursor concentration and the abundance of the gene expression machinery. Interestingly, a thorough analysis of the functioning of the ppGpp system, as described by a kinetic model of the synthesis and degradation of this signalling molecule, suggests similarities between our two-variable control strategy and the regulation of the transcription of ribosomal RNA by ppGpp [17].

The results presented here generalize the analysis of control strategies enabling optimal growth of microorganisms from steady-state to dynamical scenarios. The control strategies are formulated in the context of a coarse-grained model of resource allocation, based on minimal assumptions, that accounts for empirical growth laws at steady state. The analysis shows that during growth transitions, control strategies based on information of a single variable are outperformed by systems measuring several variables. This conclusion agrees with the intuition that, in dynamical environments, there may be an evolutionary pressure towards more elaborate sensory systems. From a methodological point of view, our study illustrates how optimal control theory can provide novel insights into complex biological phenomena [33].

2.3 Results

2.4 Self-replicator model of resource allocation

Resource allocation in bacteria involves the distribution of cellular resources (precursor metabolites and energy) over processes supporting maintenance and growth [1]. A simple modelling tool for analyzing resource allocation questions in a precise way are so-called self-replicator models. These models have a long history in various domains of chemistry, biology, physics, and computer science [34], and were recently put to use as an analytical tool in systems biology [11] (see also [35]). We will show that despite their simplicity, which make them tractable for mathematical analysis, self-replicator models are sufficiently expressive to account for empirical observations and make testable predictions.

Bearing in mind that the major constituents of the cell are macromolecules (DNA, RNA, proteins), produced from precursor metabolites, a fundamental resource allocation question is the following: How much of the cellular resources are invested in the making of new macromolecules (gene expression machinery) and how much in performing other functions, in particular producing metabolic enzymes involved in the uptake of nutrients and their conversion to precursor metabolites (metabolic machinery)? In order to ad-

dress this question, we consider a self-replicating system composed of the gene expression machinery (R) and the metabolic machinery (M). The system, shown schematically in Fig. 2.1, is thus defined by two macroreactions which are conveniently written as:

$$\begin{aligned} S &\xrightarrow{V_M} P, \\ P &\xrightarrow{V_R} \alpha R + (1-\alpha) M. \end{aligned} \tag{2.1}$$

The first reaction, catalyzed by M, converts external substrates (S) into precursor metabolites (P). The second reaction, catalyzed by R, converts precursors into macromolecules (R and M). The resource allocation parameter $\alpha \in [0, 1]$ defines the proportion of precursor mass used for making gene expression machinery as compared to metabolic machinery. We will interchangeably use the symbols M, R, S, and P for the components of the replicators themselves and their total mass [g]. We will denote the rates at which the macroreactions occur by V_R and V_M [g h^{-1}].

The self-replicator system in Fig. 2.1 is based on a number of simplifying assumptions. First, cell division is not explicitly modelled and replication should therefore be interpreted as the growth of (the mass of) a cell population. This amounts to the assumption that individual cells in a growing populations have the same macromolecular composition. Second, degradation of the macromolecules is ignored. In other words, we assume that macromolecules are stable and that their degradation rates are negligible with respect to the rates of other reactions in the system. Third, we consider only two classes of macromolecules (R and M). In particular, we do not assume that an irreducible mass fraction of the precursors is dedicated to cell maintenance [12]. The system could be easily extended to relax the above assumptions, but this would complicate the analysis of the model and obscure the points we want to make.

In what follows, it will be more convenient to describe the quantities in the system as intracellular concentrations rather than as the total mass in the cell population. To this end, we define the volume `Vol` [L] of the cell population as follows:

$$\texttt{Vol} = \beta\,(M + R), \tag{2.2}$$

with β a conversion constant [L g^{-1}] equal to the inverse of the cytoplasmic density. Dividing each variable M, R, and P by `Vol` yields the concentrations m, r, and p of metabolic enzymes, ribosomes and other components of the gene expression machinery, and precursor metabolites, respectively [g L^{-1}]. Henceforth, these variables as well as `Vol` and α will be considered functions of time t [h].

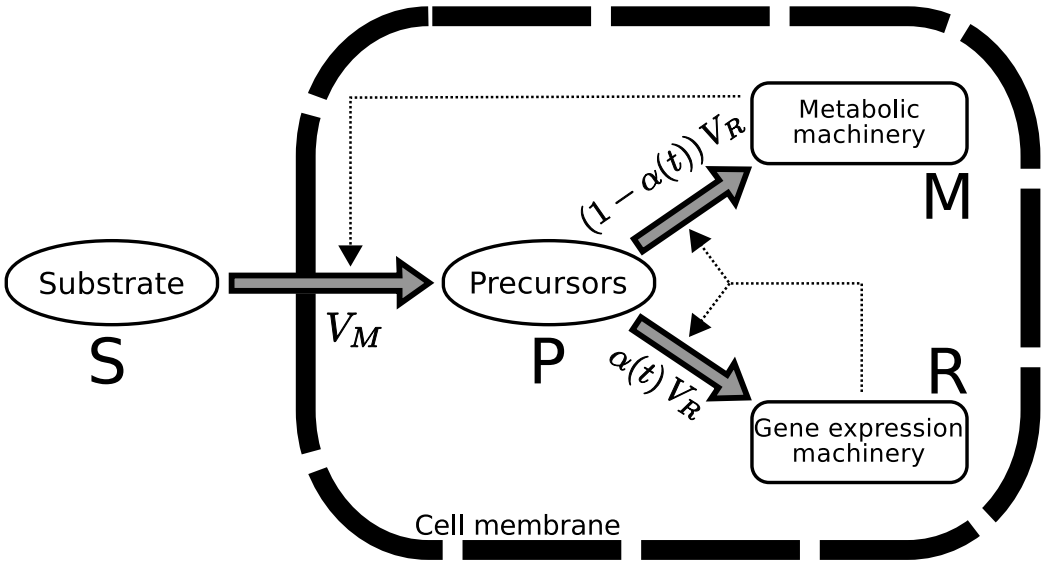

Figure 2.1 – **Self-replicator model of bacterial growth.** External substrates S enter the cell and are transformed into precursors P through the action of the metabolic machinery M. The precursors are used by the gene expression machinery R to make the proteins composing both the metabolic machinery (transporters, enzymes, ...) and the gene expression machinery itself (RNA polymerase, ribosomes, ...). α $(1-\alpha)$ is the mass proportion of precursors converted into R (M). Thick arrows denote reactions and thin, dashed arrows denote catalytic activities. The rate of synthesis of precursors and the rate of synthesis of proteins from precursors are denoted by V_M and V_R, respectively.

The dynamics of the self-replicator in Fig. 2.1 can be described by the following system of ordinary differential equations (see S1 Text for the derivation):

$$\frac{dp}{dt} = v_M(s,r) - v_R(p,r)\,(1+\beta\,p), \tag{2.3}$$

$$\frac{dr}{dt} = v_R(p,r)\,(\alpha(t)-\beta\,r), \tag{2.4}$$

where s [g L^{-1}] denote the (extracellular) concentration of substrate. $v_M(s,r)$ [g L^{-1} h^{-1}] and $v_R(p,r)$ [g L^{-1} h^{-1}] denote the precursor synthesis rate and the macromolecule synthesis rate, respectively. The growth rate μ [h^{-1}] of the replicator system is defined as the relative increase of the volume, and can be rewritten with Eqs 2.3-2.4 as proportional to the macromolecule synthesis

rate (S1 Text):

$$\mu = \frac{1}{\texttt{Vol}}\frac{d\texttt{Vol}}{dt} = \frac{1}{M+R}\frac{d(M+R)}{dt} = \beta\, v_R(p,r). \tag{2.5}$$

The precursor concentration changes through the joint effect of the precursor synthesis rate $v_M(\cdot)$, the macromolecule synthesis rate $v_R(\cdot)$, and the rate of growth dilution $(\beta\, v_R(\cdot)\, p)$. The change in concentration of ribosomes and other components of the gene expression machinery is the net effect of the ribosome synthesis rate $(\alpha(\cdot)\, v_R(\cdot))$ and the rate of growth dilution $(\beta\, v_R(\cdot)\, r)$. Remark that it is not necessary to add an equation for m because it follows from Eq. 2.2 that $r + m = 1/\beta$, and therefore $dm/dt = -dr/dt$.

We use Michaelis-Menten kinetics to define the synthesis rate of each reaction:

$$v_M(s,r) = k_M\, m\, \frac{s}{K_M + s} = k_M\, (1/\beta - r)\, \frac{s}{K_M + s}, \tag{2.6}$$

$$v_R(p,r) = k_R\, r\, \frac{p}{K_R + p}, \tag{2.7}$$

with rate constants k_M, k_R [h^{-1}] and half-saturation constants K_M, K_R [g L^{-1}]. Note that the rate of precursor synthesis is proportional to the concentration of the components of the metabolic machinery, while the macromolecule synthesis rate is proportional to the concentration of the components of the gene expression machinery. These catalytic effects correspond to the dashed arrows in Fig. 2.1. The rate constant k_M depends both on the quality of the nutrients in the medium (higher k_M for a richer medium) and on the metabolic efficiency of the macroreaction converting the substrate into precursors (higher k_M for a more efficient reaction). For convenience, we henceforth assume that the environmental conditions do not change over the time-interval considered, either because s is constant or because $s \gg K_M$, corresponding to a situation in which the substrate is available in excess. In both cases, $e_M(s) = k_M\, s/(K_M + s)$ is approximately constant, so that we can write

$$v_M(r) = e_M\, (1/\beta - r). \tag{2.8}$$

The rate constant k_R characterizes the efficiency of the gene expression machinery, depending on the elongation rate of ribosomes, among other things. The ratio p/K_R is an indicator of the saturation of the gene expression machinery by precursors.

The system of Eqs 2.3-2.4 thus has four parameters (e_M, k_R, K_R, β), one of which characterizes the input from the environment (e_M). The order of magnitude of the parameters can be inferred from data in the literature, as

explained in S2 Text. Below we use the following values for the parameters $e_M = 3.6$ h^{-1}, $k_R = 3.6$ h^{-1}, $K_R = 1$ g L^{-1}, $\beta = 0.003$ L g^{-1} (S1 Table). However, it should be emphasized that the conclusions of this paper do not depend on the exact quantitative values of these parameters.

An interesting property of the model is that it is built on minimal assumptions, basically the two macroreactions and the definition of the volume as proportional to the total mass of macromolecules. Like in [11, 13, 25], these assumptions directly lead to the expression of the growth rate in Eq. 2.5, without additional assumptions.

2.5 Growth-rate maximization of the self-replicator reproduces bacterial growth laws

The nullcline for r is given by $r = 0$, $r = \alpha/\beta$, and $p = 0$, while the nullcline for p is defined by

$$r = \frac{e_M}{\beta\left(e_M + k_R \frac{p}{K_R+p}(1+\beta p)\right)}.$$

The nullclines define a single stable steady state (p^*, r^*) (Fig. 2.2*A* and *Methods*). At this steady state, the growth rate is constant and denoted by μ^*. The nullcline for p is defined by the environment e_M. The nullcline for r, and thus the location of the steady state with the associated growth rate, are given by α. Fig. 2.2*B* shows the dependency of the steady-state growth rate μ^* on the resource allocation parameter α. As can be seen, μ^* is maximal for a specific, unique value of α, which we denote α^*_{opt}. That is, the model predicts that there is a single optimal way to divide the precursor flux over the synthesis of the gene expression machinery and the metabolic machinery. The same result, using a similar model, was obtained by Scott *et al.* [13]. The self-replicator model is simple enough to derive an algebraic expression for computing α^*_{opt} and the corresponding maximal growth rate μ^*_{opt} (*Methods* and S1 Text), which will simplify analysis of the system in later sections.

In order to validate the model, we verified that it can account for data on the macromolecular composition of *E. coli* at steady state [12]. When optimizing α for different values of e_M (assuming cells attain maximal growth), the model predicts a relation between α^*_{opt} and μ^*_{opt} (colored dots and black dashed line in Fig. 2.3*A*) that is quasi-linear for high growth rates. We compared this prediction with the results of experiments where the relation between the growth rate and the mass ratio of total RNA and protein was determined in different growth media (Fig. 2.3*B*). In the framework of our

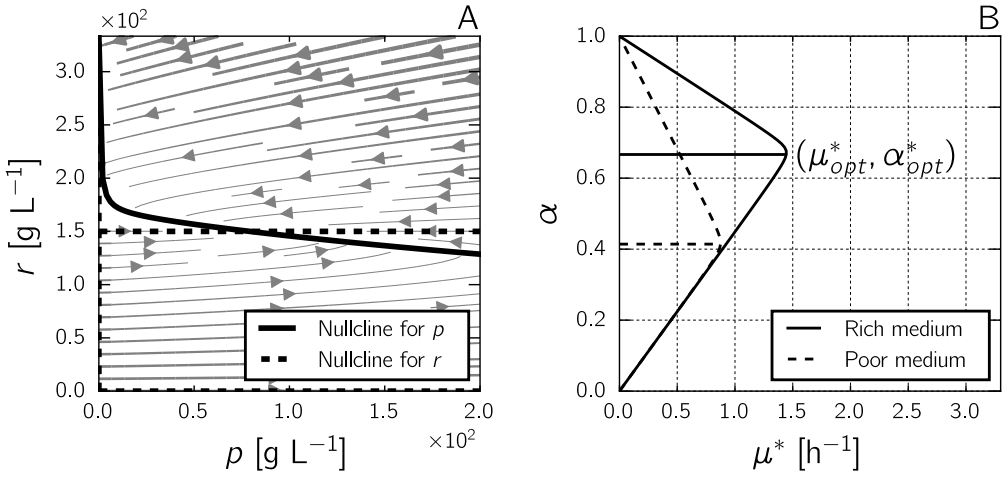

Figure 2.2 – **Analysis of self-replicator model of bacterial growth.** *A:* Phase-plane analysis of the self-replicator model of Eqs 2.3 and 2.4. The nullclines for p and r are shown as solid and dashed curves, respectively. Parameter values are $e_M = 3.6$ h^{-1}, $k_R = 3.6$ h^{-1}, $K_R = 1$ g L^{-1}, $\beta = 0.003$ L g^{-1}, $\alpha = 0.45$. *B:* Dependence of the growth rate at steady state μ^* on the resource allocation parameter α, for two different environmental conditions (solid line, $e_M = 4.76$ h^{-1}; dashed line, $e_M = 1.57$ h^{-1}, other parameter values are $k_R = 2.23$ h^{-1}, $K_R = 1$ g L^{-1}, and $\beta = 0.003$ L g^{-1}). The maximal growth rate is attained for a unique α, called α^*_{opt}.

model, different media correspond to different values of e_M, and different total RNA/protein mass ratios to different values of α (up to a conversion factor), allowing a direct comparison of the model predictions in Fig. 2.3*A* with the data in Fig. 2.3*B* (see *Methods*). As can be seen, the model is able to account for the observed quasi-linear relation between the growth rate and the total mass ratio of RNA and protein. Moreover, for realistic values of k_R and e_M, a good quantitative fit is obtained (*Methods* and S1 Table).

The data from Scott *et al.* also reveal a second apparently linear relation between the growth rate and the total RNA/protein mass ratio. This relation is obtained when varying, in the same growth medium, the efficiency of protein synthesis by adding different doses of an inhibitor of translation (chloramphenicol) [12]. Using the model, we computed α^*_{opt} and μ^*_{opt}, for constant environment e_M and different values of the efficiency of protein synthesis k_R (dashed colored lines in Fig. 2.3*A*). As can be seen in Fig. 2.3*B*, the model also captures the second linear relation in the data.

We conclude that the self-replicator model is able to reproduce known

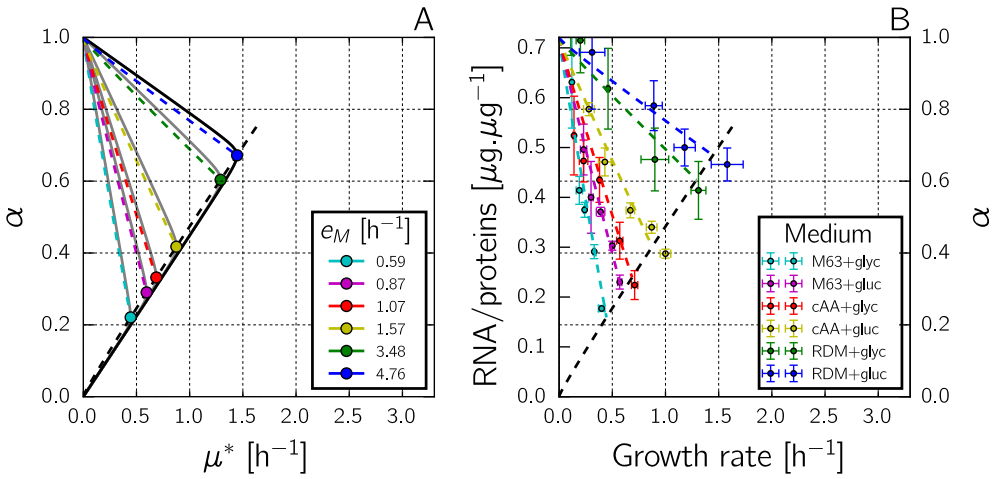

Figure 2.3 – **Self-replicator model accounts for bacterial growth laws.** *A:* Predicted quasi-linear relation between the maximal growth rate μ^*_{opt} and the corresponding optimal resource allocation α^*_{opt}, for different values of e_M (different colors). The colored dots indicate α^*_{opt} and μ^*_{opt} for $k_R = 2.23$ h^{-1} and different e_M, and the dashed black line the relation for all intermediate values of e_M. The dashed colored lines indicate the relation between α^*_{opt} and μ^*_{opt} obtained when, for a given value of e_M, the value of k_R is decreased (lower k_R leads to lower μ^*_{opt}). The solid grey curves correspond to (μ^*, α)-profiles like those shown in Fig. 2.2*B*. *B:* Measured relation between the total RNA/protein mass ratio and the growth rate, in different growth media with different doses of a translation inhibitor (data from [12]). For each medium, indicated by a color, five different concentrations of inhibitor were used (higher dose leads to lower growth rate). Growth-medium compositions are given in the original publication and error bars represent standard deviations. The dashed black and colored lines are the same as in panel *A*, indicating the good quantitative correspondence between model predictions and experimental data for the chosen parameter values, obtained by fitting the model to the data points (see *Methods* for details).

observations of resource allocation in bacteria, so-called growth laws [12]. The model is similar to a model recently proposed by Scott *et al.* [13]. Contrary to the latter model, the translation rate is not assumed to be constant in the self-replicator model, but rather depends on precursor abundance, as proposed by the same authors in [36].

The above analysis of bacterial growth has two major limitations. First, the predictions of optimal resource allocation (the value of α leading to

the maximal growth rate) hold at steady state, for a constant environment, whereas most bacteria are not expected to encounter such conditions outside the laboratory. An allocation of resources that is optimal for steady-state growth and constant over time may not be optimal in dynamical growth conditions. Second, while it predicts which value of α is optimal at steady state, the model says nothing about the strategies that could be used to control resource allocation and set α to its optimal value. In other words, how could bacterial cells use sensors of changes in their internal state and the environment to optimally adjust α? In what follows, we will address the above two questions, after having given a precise statement of the problem of optimal resource allocation in a dynamical environment in the next section.

2.6 Biomass maximization as an optimal control problem

A self-replicator at steady state accumulates biomass according to $\texttt{Vol}(0)\, e^{\mu^* t}$, $t \in [0, \tau]$, when μ^* is the growth rate at steady state. The accumulation of biomass is obviously maximal when the growth rate is maximal ($\mu^* = \mu^*_{opt}$). In dynamical conditions, the growth rate is not constant and biomass accumulation is described more generally by:

$$\frac{d\texttt{Vol}}{dt} = \mu(t)\, \texttt{Vol}.$$

In other words, when integrating over the time interval $[0, \tau]$:

$$\ln\left(\frac{\texttt{Vol}(\tau)}{\texttt{Vol}(0)}\right) = \int_0^\tau \mu(t)\, dt. \tag{2.9}$$

Since the logarithm is an increasing function, maximizing the biomass produced over $[0, \tau]$ requires maximization of the right-hand side of the equation.

In a changing environment, maximization of the integral in Eq. 2.9 will generally require the optimal value of α to be a function of time instead of a specific constant value. This dynamical resource allocation problem can be formulated in a more precise way using concepts from optimal control theory [29]. Let J be the objective function

$$J(\alpha) = \int_0^\tau \mu(t)\, dt = \int_0^\tau \beta\, v_R(p, r)\, dt,$$

where $\alpha : \mathbb{R}^+ \to [0, 1]$ is a time-dependent function. The time evolution of p and r is determined by the self-replicator model of Eqs 2.3 and 2.4, and p

and r thus depend on e_M and α. Moreover, let $\mathcal{U} = \{\alpha : \mathbb{R}^+ \to [0,1]\}$ be the set of admissible controls. The optimal dynamical control problem then consists in finding the time-varying function $\alpha_{opt}(t)$ that maximizes $J(\alpha)$ over the time-interval $[0,\tau]$:

$$\alpha_{opt} = \arg\max_{\alpha\in\mathcal{U}} J(\alpha). \tag{2.10}$$

In what follows, we will simplify the above problem by considering that the environment changes in a step-wise fashion at $t = 0$, but remains constant over the time-interval $[0,\tau]$, that is, $e_M(t) = e_M$. More specifically, we focus on the case of a nutrient upshift, corresponding to a step-wise increase of e_M. This upshift scenario corresponds to classical experiments in bacterial physiology [37–39], reviewed in [28], and is frequently encountered in the life cycle of a microorganism [1]. Notice that more complex environments can be approximated by a sequence of step-wise nutrient upshifts and downshifts.

2.7 Solution of the optimal control problem

Optimal dynamical control problems for two-dimensional nonlinear dynamical systems, like the problem of Eq. 2.10, are generally difficult to solve. However, we will show that the class of functions to which α_{opt} belongs can be identified, and we will use numerical optimization to identify a particular α_{opt} maximizing J.

As a preliminary step, in order to simplify the analysis, the variables in the self-replicator model of Eqs 2.3 and 2.4 are made nondimensional, by defining $\hat{t} = k_R\, t$, $\hat{p} = \beta\, p$, and $\hat{r} = \beta\, r$. This leads to the following ODE system:

$$\frac{d\hat{p}}{d\hat{t}} = (1-\hat{r})\, E_M - (1+\hat{p})\,\hat{r}\,\frac{\hat{p}}{K+\hat{p}}, \tag{2.11}$$

$$\frac{d\hat{r}}{d\hat{t}} = \hat{r}\frac{\hat{p}}{K+\hat{p}}\,(\alpha(\hat{t}) - \hat{r}), \tag{2.12}$$

where $K = \beta\, K_R$ and $E_M = e_M/k_R$. The nondimensional growth rate is given by:

$$\hat{\mu} = \frac{\mu}{k_R} = \frac{\hat{p}}{K+\hat{p}}\,\hat{r}. \tag{2.13}$$

Notice that the nondimensionalized system depends on a single parameter K, in addition to the constant environment E_M, which functions as an input to the system.

Analysis of the nondimensionalized system allows a number of properties of the solution of the optimal control problem of Eq. 2.10 to be derived (*Methods* and S3 Text). First, by applying a version of the well-known Pontryagin Maximum Principle [40], we can prove that the optimal solution is obtained for an alternating sequence of $\alpha(\cdot) = 0$ and $\alpha(\cdot) = 1$, possibly ending with an intermediate value of $\alpha(\cdot)$, corresponding to the optimal steady state $(\hat{p}(t), \hat{r}(t)) = (\hat{p}^*_{opt}, \hat{r}^*_{opt})$, that is, the steady state leading to the optimal growth rate $\hat{\mu}^*_{opt}$ in the post-upshift environment E_M. Second, if the optimal solution reaches the optimal steady state for the new environment, then it does so after an infinite number of switches of $\alpha(\cdot)$ between 0 and 1. Third, this switching behavior is characterized by a so-called switching curve $\hat{r} = \varphi(\hat{p})$ in the $(\hat{p}, \hat{r})$-plane, which passes through $(\hat{p}^*_{opt}, \hat{r}^*_{opt})$. The switching curve divides the phase plane into two regions, such that $\alpha(\cdot)$ switches to 0 when the system is in the region above φ and to 1 when the system is below φ (black dashed curve in Fig. 2.4*A*).

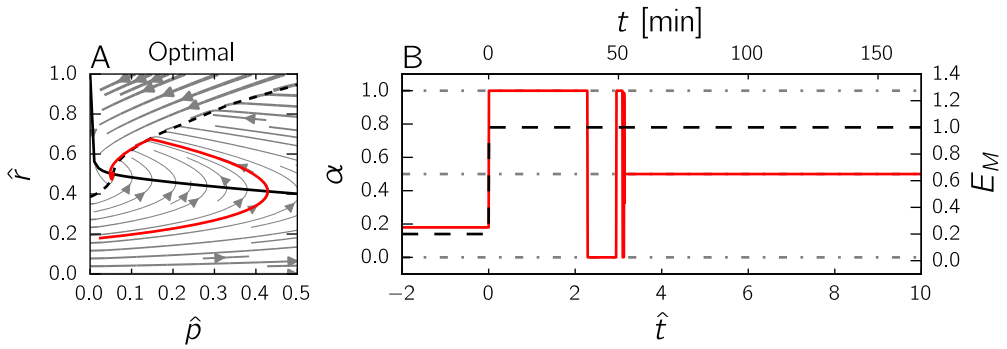

Figure 2.4 – **Optimal control of the self-replicator during a nutrient upshift.**
A: Optimal trajectory in the phase plane for the nondimensionalized model of Eqs 2.11-2.12, with streamlines. The optimal trajectory is shown as a solid, red curve. The solid, black curve represents the $\hat{p}$-nullcline. The dashed, black curve is the switching curve $\varphi(\hat{p})$. The optimal solution was obtained by numerical optimization using `bocop` [41] (see *Methods* for details), using the parameter values $E_M = 1$ and $K = 0.003$, and starting from the initial state $(0.024, 0.18)$ at $t = 0$ (optimal steady state for $E_M = 0.2$). *B:* Time evolution of the control variable $\alpha_{opt}(\cdot)$ (thick, red line) and the environment E_M (dashed, black line).

In line with these results, we conjecture that the optimal solution consists in a switching transient towards the optimal steady state for the new

environment, and remains at this steady state until the next environmental change. Such a solution is known as a bang-bang-singular solution in the control theory literature [29]. Formally, the solution of Eq. 2.10 can be described as

$$\alpha_{opt}(\hat{t}) = \begin{cases} 0, \text{ if } \hat{r}(\hat{t}) > \varphi(\hat{p}(\hat{t})), \\ 1, \text{ if } \hat{r}(\hat{t}) < \varphi(\hat{p}(\hat{t})), \\ \alpha^*_{opt}, \text{ if } (\hat{p}(\hat{t}), \hat{r}(\hat{t})) = (\hat{p}^*_{opt}, \hat{r}^*_{opt}). \end{cases} \tag{2.14}$$

Notice that the optimal solution involves dynamical feedback from the state of the system to the control variable $\alpha(\cdot)$, and is therefore an instance of closed-loop optimization [29].

The optimal control problem of Eq. 2.10 was also solved numerically by a direct method using the `bocop` software [41] (see *Methods* for details). A time discretization allows the problem to be transformed into a nonlinear optimization problem solved here by interior point techniques. The optimal trajectories obtained numerically confirm our conjecture that the optimal control is bang-bang-singular. An example solution, obtained by numerical optimization is shown in Fig. 2.4. At time $\hat{t} = 0$, E_M jumps from a low to a high value, corresponding to a nutrient upshift (dashed black line in Fig. 2.4B). The optimal solution α_{opt} consists of a sequence of switches between $\alpha = 1$, corresponding to maximal synthesis of the gene expression machinery, and $\alpha = 0$, corresponding to maximal synthesis of the metabolic machinery, until $(\hat{p}^*_{opt}, \hat{r}^*_{opt})$ is reached. α is then set to α^*_{opt}, the value leading to the maximum growth rate in the new medium (here 0.5, for $E_M = 1$). The sequence of switches of α in Fig. 2.4*B* corresponds to successive crossings of the switching curve in Fig. 2.4*A*. In particular, the switch just after $\hat{t} = 2$ corresponds to the first crossing of the switching curve; the subsequent switches accumulate around the steady state and are therefore difficult to identify in the plot.

What is the biological relevance of the bang-bang-singular solution maximizing growth of the bacterial self-replicator? In order to answer this question, we will investigate in the next two sections the different ways in which microorganisms could implement or have been shown to implement feedback growth control by sensing the environment and cellular physiology. Although the idealized solution proposed by optimal control theory will obviously not be found in nature, actual control strategies may produce solutions that are close. The optimal solution can thus be used as a gold standard, a benchmark for comparing actual control strategies.

2.8 Simple feedback control strategies: exploiting information on nutrients or precursors

The control strategies that microbial cells have evolved to bring resource allocation in line with changes in the environment involve a variety of molecular mechanisms [42]. These mechanisms are responsible for sensing the environment and the physiological state of the cell, as well as for adjusting the expression of genes that encode components of the transcriptional and translational machinery, enzymes, transporters, and proteins with other metabolic functions.

In the framework of the self-replicator model of bacterial growth, control strategies take the form of feedback control laws mapping the value of system variables to a value of the control variable $\alpha(\cdot)$. In this section, we explore two such strategies, the first exploiting information on the quality and quantity of substrate present in the environment, as reflected in the value of E_M, and the second using information on the precursor concentration $\hat{p}$. The feedback control strategies are graphically displayed in Fig. 2.5, as an extension of the self-replicator of Fig. 2.1. We pose a number of mathematical constraints on the feedback control strategies considered below. First, we require the control laws to be functions of the variables of the self-replicator but not involve derivatives or integrals of these variables. Second, for a constant environment E_M, the control strategies must drive the system to a unique stable and non-trivial steady state, enabling a non-zero growth rate. Third, this steady state must equal the optimal steady state for that environment, given by $(\hat{p}^*_{opt}, \hat{r}^*_{opt})$.

The first control strategy is defined by the function $f\colon \mathbb{R}^+ \to [0,1]$, mapping E_M to α:

$$\alpha = f(E_M). \tag{2.15}$$

Notice that α is constant because E_M is fixed to the value defining the new environment after the upshift. What would be an appropriate choice for f? An advantage of the self-replicator model is that the optimal allocation at steady state can be explicitly formulated as a function of E_M (Eq. 2.22 in *Methods*, with derivation in S1 Text). This function is the unique function satisfying all of the above criteria (S1 Text). S1 Figure plots f and shows that it is conveniently approximated by a Michaelis-Menten function, *i.e.*,

$$\alpha(\cdot) = \frac{E_M}{E_M + K_{mE}}, \tag{2.16}$$

with the dimensionless half-saturation constant K_{mE}. The interest of the approximation is that it demonstrates that the control strategy can be described by a simple and ubiquitous response curve in biochemical kinetics.

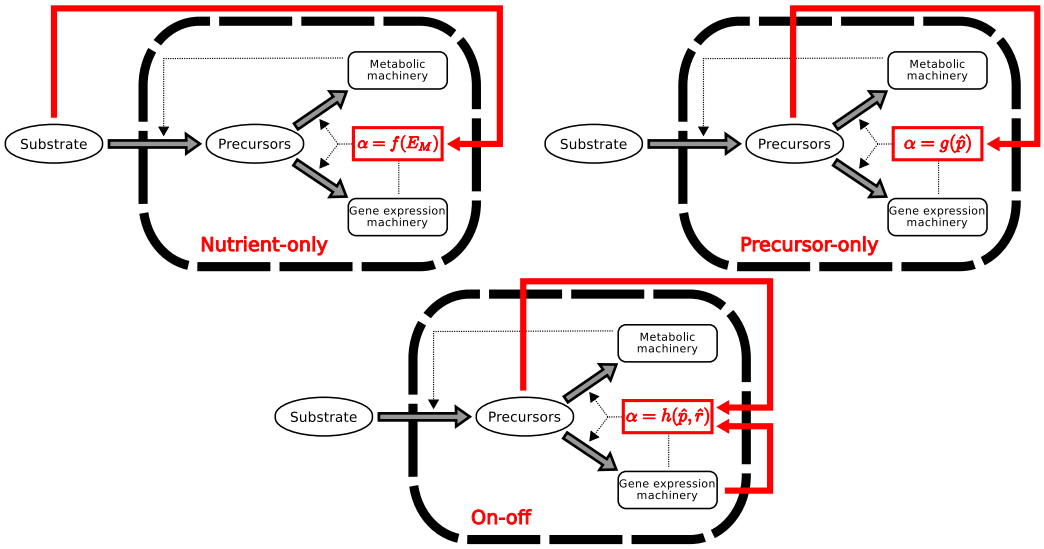

Figure 2.5 – **Alternative strategies for controlling the self-replicator of bacterial growth.**
The feedback control strategies, shown in red and superposed on the self-replicator of Fig. 2.1, exploit information on system variables and the environment to adjust the value of α, and thus the relative allocation of resources to the metabolic machinery and gene expression machinery.

As an example of a regulatory system resembling the above control strategy consider the phosphotransferase system responsible for the uptake of glucose, the preferred substrate of *E. coli* [43]. In the presence of glucose, the EIIA^{Glc} component of the phosphotransferase system is mostly unphosphorylated, since the phosphate groups are used for the conversion of extracellular glucose to intracellular glucose-6-phosphate. When glucose disappears from the medium, however, the glucose uptake rate decreases and, correspondingly, the phosphorylated fraction of EIIA^{Glc} increases. The phosphorylation state of EIIA^{Glc} thus provides an indirect read-out of glucose availability. In response to this signal, a variety of metabolic processes are upregulated or downregulated, notably involving the signalling molecule cAMP which activates the pleiotropic transcription factor Crp [43, 44].

How does the control strategy of Eq. 2.15, which we call a nutrient-only strategy, perform in comparison with the optimal solution derived in the previous section? That is, how much biomass does this strategy produce compared with the maximal amount of biomass that can theoretically be obtained after a nutrient upshift? In order to answer these questions, we simulated the response to a sudden upshift of the self-replicator of Eqs 2.11-2.12

controlled by the nutrient-only strategy of Eq. 2.15. The results are shown in Fig. 2.6. Panel A shows the trajectory of the controlled self-replicator system and panel D plots the evolution of the amount of biomass as a fraction of the amount of biomass produced by the optimal strategy. While the system does reach the steady state that is optimal for E_M, the nutrient-only strategy has poor performance in the transient phase immediately following the nutrient upshift. As can be seen from the solution trajectory in Fig. 2.6A, fixing α to the value that enables optimal growth at steady state leads to a huge transient overshoot of the precursor concentration. The overshoot reveals that resource allocation is initially suboptimal, with too many resources invested in the metabolic machinery at the expense of the gene expression machinery. This causes a transiently suboptimal growth rate, leading to lower biomass accumulation (Eq. 2.9).

One way to avoid the transient precursor imbalance observed in Fig. 2.6A would be to exploit information on the precursor concentration in the control strategy. The second strategy considered here, which we label a precursor-only strategy, does exactly this: it involves a feedback control law $g\colon \mathbb{R}^+ \to [0,1]$ mapping $\hat{p}$ to α:

$$\alpha = g(\hat{p}). \tag{2.17}$$

Since $\hat{p}$ will vary during the upshift experiment, α is not constant, contrary to the nutrient-only strategy above. In the *Methods* section, we present a function g satisfying the requirements listed in the beginning of this section, in particular that the system converge to a stable steady state ensuring maximal growth in the new environment. Moreover, we show that any other choice for g leads to lower biomass production. The function is plotted in S1 Figure, and as shown in the same panel, is conveniently approximated by a Hill function with cooperativity coefficient 2:

$$\alpha(\cdot) = \frac{\hat{p}^2}{\hat{p}^2 + {K_{mp}}^2}, \tag{2.18}$$

where K_{mp} is a dimensionless half-saturation constant.

While converging to the same steady state, this second strategy, which we will refer to as the precursor-only strategy, performs much better than the nutrient-only strategy after an upshift, as shown in Fig. 2.6. We simulated the response to a nutrient upshift of the self-replicator of Eqs 2.11-2.12 with the precursor-only strategy of Eq. 2.17. The relative biomass increases by 51% and reaches 94% of the biomass produced by the optimal control strategy (the theoretical maximum). The precursor-only strategy notably avoids the inefficient transient accumulation of precursors directly after the

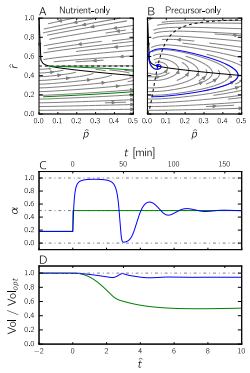

Figure 2.6 – **Comparison of the performance of the nutrient-only and precursor-only strategies after a nutrient upshift.**
A: Trajectory in the phase plane for the nutrient-only strategy (green curve). The solid, black curve represents the $\hat{p}$-nullcline. The dashed, black curve is the $\hat{r}$-nullcline. The solution is obtained by numerical simulation of the system of Eqs 2.11-2.12, supplemented with $\alpha = f(E_M)$ as specified by Eq. 2.27 in the *Methods* section and plotted in S1 Figure. The initial state corresponds to the steady state attained for an environment given by $0.2\,E_M$. While converging to the new steady state after the upshift, the precursor concentration makes a large overshoot. *B:* As above, but for the precursor-only strategy. The feedback control strategy is now defined by $\alpha = g(\hat{p})$ as specified by Eq. 2.28 in the *Methods* section and plotted in S1 Figure. The solution trajectory (blue curve) exhibits a lower overshoot. *C:* Evolution of the control variable $\alpha(\cdot)$ as a function of time, for each of the above two strategies. Notice that in the nutrient-only strategy $\alpha(\cdot)$ immediately jumps to the optimal value for the post-upshift steady state (green curve), whereas in the precursor-only strategy it depends on the (time-varying) precursor concentration (blue curve). *D:* Evolution of the ratio $\texttt{Vol}/\texttt{Vol}_{opt}$ as a function of time, where $\texttt{Vol}$ is the volume of the self-replicator and $\texttt{Vol}_{opt}$ the volume of the same replicator following the optimal strategy shown in Fig. 2.4. In all of the above simulations, the parameter values $E_M = 1$ and $K = 0.003$ were used.

nutrient upshift, by alternatingly investing more resources in gene expression (consumption of precursors) and metabolism (production of precursors). In this respect, the oscillatory time profile of α (Fig. 2.6*C*) is somewhat reminiscent of the bang-bang-singular control in the solution of the optimal control problem (Fig. 2.4*B*).

Both strategies, nutrient-only and precursor-only, drive the self-replicator towards the same steady state. Whereas the two strategies are thus indistin-

guishable when the analysis is restricted to steady state, the precursor-only strategy is shown to perform much better in a dynamical upshift scenario, in the sense that the biomass produced is much closer to that produced by the optimal strategy. Several authors have concluded that control strategies based on precursor sensing are key for maintaining optimal growth at steady state. Scott *et al.* argue that a strategy similar to the precursor-only approach above allows robust control of amino acid supply and demand, resulting in optimal steady-state growth over a range of nutrient conditions [13]. They associate this strategy with ppGpp-mediated control of the synthesis of ribosomal proteins [30–32]. The signalling molecule ppGpp accumulates in response to an increase in the level of uncharged tRNA, when amino acid concentrations in the cell drop. This causes ribosomes to "stall" and leads to RelA-mediated conversion of GTP to ppGpp, the molecular details of which are still subject of debate [32, 45]. Since ppGpp inhibits the transcription of ribosomal RNAs [46], the concentration of the latter decreases, leading to more inactive ribosomal proteins and, through a well-characterized post-transcriptional autoregulatory mechanism, a lower synthesis rate of ribosomal proteins [31, 47]. Our analysis adds to the above study a novel insight: measuring precursors does not only enable resource allocation control to achieve maximal growth at steady state, but is also a good strategy in a dynamical context.

While the precursor-only strategy is thus seen to lead to good results, Fig. 2.6*D* shows that there remains room for improvement. It seems reasonable to expect that control strategies exploiting information of not just a single variable, but several variables simultaneously, could further improve the performance of the self-replicator during a growth transition.

2.9 A near-optimal feedback control strategy: exploiting information on the imbalance between precursors and the gene expression machinery

In the quest for further improvements, a natural starting-point would be to consider the curve defining the optimal steady states $(\hat{p}^*_{opt}, \hat{r}^*_{opt})$ for different environments E_M. This curve is defined by a function mapping $\hat{p}^*$ to $\hat{r}^*$, which is actually the same as the function g introduced in the precursor-only strategy (*Methods* and S1 Figure), given that at steady state $\hat{r} = \alpha$ (Eq. 2.12). The curve can be seen as representing an optimal balance

between precursors and the gene expression machinery, in the sense that the maximal growth rate attainable for a given precursor concentration $\hat{p}$ requires a concentration $\hat{r}$ of ribosomes and other components of the gene expression machinery equal to $g(\hat{p})$. If either $\hat{r} > g(\hat{p})$ or $\hat{r} < g(\hat{p})$, the growth rate is suboptimal.

These considerations suggest an intuitive control strategy, namely to avoid an imbalance between $\hat{p}$ and $\hat{r}$ at all times, and remain as close as possible to the curve defined by g. In particular, when the gene expression machinery is more abundant than what is optimal given the available precursors ($\hat{r} > g(\hat{p})$), its synthesis is switched off ($\alpha = 0$). Conversely, when $\hat{r} < g(\hat{p})$, synthesis of the gene expression machinery is switched on. This strategy thus tries to restore "as quickly as possible" the optimal balance between precursors $\hat{p}$ and the gene expression machinery $\hat{r}$, giving rise to a so-called on-off control strategy:

$$\alpha = h(\hat{p}, \hat{r}) = \begin{cases} 0, \text{ if } \hat{r} > g(\hat{p}), \\ 1, \text{ if } \hat{r} < g(\hat{p}), \\ \alpha^*_{opt} \text{ if } (\hat{p}, \hat{r}) = (\hat{p}^*_{opt}, \hat{r}^*_{opt}). \end{cases} \tag{2.19}$$

As shown in the *Methods* section, the on-off strategy drives the system to a stable steady state ensuring growth at the maximal rate. Notice that, contrary to the strategies discussed in the previous section, the value of α selected by the on-off strategy depends on both $\hat{p}$ and $\hat{r}$ (Fig. 2.5). It thus uses more information on the state of the system than the nutrient-only and precursor-only strategies.

Fig. 2.7 shows the performance of the on-off strategy after a nutrient upshift, as compared to the precursor-only strategy. The transition is seen to be nearly perfect, in the sense that 98% of the optimal biomass is produced by the strategy. The time course of α in panel D is very similar to the optimal time course obtained by numerical optimization, shown in Fig. 2.4*B*, and clearly brings out the bang-bang-singular nature of the solution. These results show that a strategy exploiting complete information on the internal state of the self-replicator can lead to near-optimal performance, outcompeting a strategy that uses partial information on the internal state (precursor abundance only).

Are microbial cells equipped with mechanisms implementing a strategy similar to the on-off strategy? A possible candidate would again be the ppGpp system. A kinetic model of ppGpp metabolism and the regulation of the synthesis of ribosomal proteins was recently presented by Bosdriesz *et al.* [17]. The model proved capable of accounting for a range of experimental data, including the steady-state concentration of ppGpp as a function of the

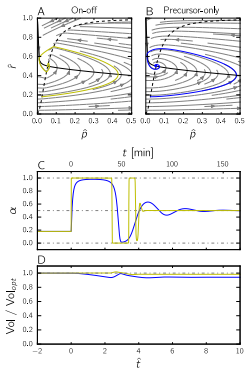

Figure 2.7 – **Comparison of the performance of the precursor-only and the on-off strategies after a nutrient upshift.**
A: Trajectory in the phase plane for the on-off strategy (yellow curve). The solid, black curve represents the $\hat{p}$-nullcline and the dashed, black curve the function g. The solution is obtained by numerical simulation of the system of Eqs 2.11-2.12, supplemented with the equation $\alpha = h(\hat{p}, \hat{r})$ defined in Eq. 2.19 and plotted in Fig. 2.8*A*. The initial state corresponds to the optimal steady state attained for an environment given by $0.2\,E_M$. *B:* Trajectory in the phase plane for the precursor-only strategy (same as in Fig. 2.6*B*, added for comparison). *C:* Evolution of the control variable α for each strategy as a function of time. Both strategies stabilize the system at the optimal steady state, but only the on-off strategy (yellow curve) exhibits bang-bang behavior. *D:* Evolution of the ratio $\texttt{Vol}/\texttt{Vol}_{opt}$ for the on-off and precursor-only strategies as a function of time, where `Vol` is the volume of the self-replicator and $\texttt{Vol}_{opt}$ the volume of the same replicator following the optimal strategy shown in Fig. 2.4. The final values of $\texttt{Vol}/\texttt{Vol}_{opt}$ attained by the two strategies are 0.9831 and 0.9413, respectively. The on-off strategy is thus hardly distinguishable from the optimal control strategy in the plot. In all of the above simulations, the parameter values $E_M = 1$ and $K = 0.003$ were used.

growth rate [48] and the dynamical response of ppGpp to a nutrient upshift or downshift [49]. A major conclusion of the model is that the steady-state concentration of ppGpp exhibits a strongly ultrasensitive response to deviations of the ribosomal protein fraction from the optimal ribosomal protein fraction at a given growth rate. These deviations from optimality, in turn, lead to a switch-like response of the synthesis rate of ribosomal proteins (Fig. 4 in Bosdriesz *et al.* [17]).

How does this mechanistic model of ppGpp regulation relate to the on-off strategy presented above? In order to answer this question, we first need to

find a correspondence between the variables p and r of our coarse-grained model and the concentrations of molecular species in the kinetic model of Bosdriesz *et al.* This is rather straightforward to achieve, by equating p to the total amino acid concentration and r to the ribosome concentration. Second, S4 Text shows that by making two simplifying assumptions, ppGpp can be expressed as a function of the total amino acid concentration and the ribosome concentration. In particular, we assume that concentrations of all individual amino acids are equal, and that the concentrations of charged tRNAs and ppGpp evolve fast relative to the dynamics of the amino acid and ribosome concentrations. The third step consists in positing an explicit relation between ppGpp and α, based on the regulatory action of ppGpp on the transcription of ribosomal RNA [46]:

$$\alpha(\cdot) = \frac{K_I}{K_I + \texttt{ppGpp}(\cdot)}, \tag{2.20}$$

with K_I a Michaelis-Menten inhibition constant [μmol L^{-1}] and `ppGpp` the (time-varying) intracellular concentration of ppGpp [μmol L^{-1}].

The response function for ppGpp thus obtained and evaluated for a range of amino acid and ribosome concentrations is represented in Fig. 2.8, and visually compared with the on-off strategy. As can be seen, the two response surfaces are very similar. In other words, the ultrasensitive response of the synthesis rate of ribosomal proteins to the suboptimal allocation of cellular resources, derived from a model of the molecular mechanisms involved in the synthesis, degradation, and regulatory action of ppGpp [17], implements a control strategy that is close to the optimal predicted by a control-theoretical analysis of the self-replicator. While the role of ppGpp in maintaining optimal resource allocation was already pointed out by Scott *et al.* and Bosdriesz *et al.*, the latter studies were restricted to optimizing steady-state growth. A major insight from the analysis in this section is that this conclusion seems to carry over to dynamical scenarios as well. Fundamentally, the analysis suggests that the ppGpp system is a likely candidate to fulfill this role because it integrates information on the imbalance between precursor concentration and abundance of the gene expression machinery.

2.10 Discussion

Quantitative growth laws are empirical regularities pointing at fundamental properties of microbial life [50]. Recent work has led to the precise theoretical formulation of growth laws and has shown that they can be derived from basic assumptions on the molecular processes responsible for the

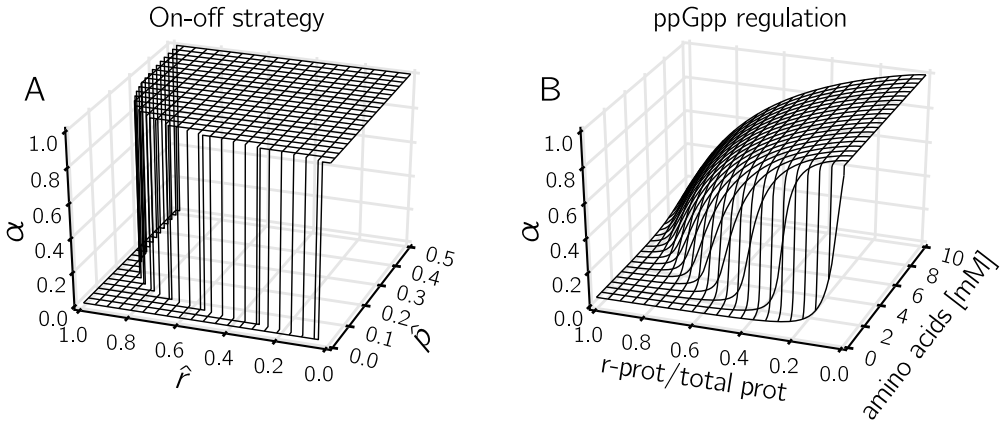

Figure 2.8 – **ppGpp regulation implements an on-off control strategy of resource allocation.**
A: Response surface of the on-off control strategy, defined by $\alpha = h(\hat{p}, \hat{r})$ in Eq. 2.19. *B:* Response surface of the ppGpp control strategy, as defined by Eq. 2.20 and the simplified kinetic model defining ppGpp in terms of the total amino acid concentration and the ribosomal protein fraction (S4 Text). The shape of the response surface of the ppGpp control strategy is seen to be in very good agreement with the on-off strategy leading to near-optimal performance of the self-replicator during a nutrient upshift.

assimilation of nutrients and their conversion to biomass [11, 13, 15, 17, 18]. The growth laws are uniquely defined under the hypothesis that microorganisms allocate resources in such a way as to maximize their growth rate. Several of the above-mentioned studies have analyzed feedback control strategies on the molecular level enabling cells to achieve optimal resource allocation in a robust manner. The control strategies exploit information on the physiological state of the cell to adjust the (relative) rate of synthesis of different classes of proteins (ribsomes, metabolic enzymes, ...). Whereas the growth laws describe microbial growth at steady state, most microorganisms live in complex, continuously changing environments. Despite some precursory work [25, 26], questions about the dynamics of microbial growth remain largely unanswered: Which resource allocation schemes are optimal in changing environments? Which dynamical control strategies lead to (near-)optimal resource allocation? How do these strategies compare with those actually implemented by microorganisms?

We have addressed the above questions by means of a self-replicator model of microbial growth, which, like other coarse-grained models of bacterial growth [11, 13, 15], is capable of reproducing the growth laws at steady state

(Fig. 2.3). A first major contribution of our work is to show that, in the case of a dynamical upshift scenario, optimal production of biomass requires a bang-bang-singular resource allocation scheme (Fig. 2.4). That is, the optimal self-replicator should iteratively allocate all of its resources to the gene expression machinery (bang control input) and the metabolic machinery (another bang control input), until the steady state enabling maximal growth in the post-upshift environment is reached, corresponding to a trade-off in the allocation of resources to the two processes (singular control input).

Bang-bang phenomena are widespread in a variety of life processes. Applications of optimal control theory to reproductive strategies in insects [51], the development of intestinal crypts [52], and the activation of metabolic pathways [53, 54] have led to bang-bang or bang-bang-singular strategies. In optimal control problems, such a solution arises with systems where the differential equations are linear in the control variable (in our case, $\alpha(\cdot)$). Examples of applications that are close to the problem considered here are the control of gene expression for adaptation to environmental changes [25, 55], and the allocation of resources between nutrient uptake and growth in microorganisms [26,56]. Whereas the former applications focus on minimization of response times, the latter also optimize biomass during a growth transition, using a different model, not derived from first principles as in this study. However, the optimal solution of the corresponding optimal control problem is also bang-bang-singular, thus showing that our conclusions are robust to model variations.

Our second major contribution is the assessment of how different feedback control strategies perform with respect to each other and to the gold standard determined from optimal control theory. We show that the precursor-only and nutrient-only strategies, both of which drive the self-replicator to the steady state with maximal growth rate in a static environment, perform quite differently in a dynamical upshift scenario (Fig. 2.6). While the precursor-only strategy is better than the nutrient-only strategy in a dynamical environment, it is in turn outperformed by a so-called on-off strategy, which achieves a near-perfect growth transition by exploiting information on the imbalance between the precursor concentration and the abundance of the gene expression machinery (Fig. 2.7). The superior performance of the on-off strategy can be intuitively explained by the fact that during a growth transition the two variables are not fully correlated, which means that sensing both instead of either one provides additional information in a dynamical context.

Interestingly, the on-off strategy is based on a feedback control law that very much resembles the response function for ppGpp-mediated regulation of the synthesis of ribosomal RNAs in *E. coli* [17]. The role of ppGpp in con-

trolling microbial growth has been amply documented [30–32]. For example, Potrykus *et al.* observed that in cells without ppGpp ($ppGpp^0$ mutants) the RNA/protein mass ratio, a proxy for our resource allocation variable α, does not change with the growth rate, which has led these authors to conclude that ppGpp is the major source of growth-rate control in *E. coli* [57]. The central importance of ppGpp in the reallocation of gene expression resources in *E. coli* following changes in nutrient availability has also been mapped with higher resolution, using genome-wide transcriptome studies [58, 59]. In nearly all bacterial species examined so far, ppGpp is known to accumulate in response to an increase in the level of uncharged tRNA [60], although the molecular details of ppGpp metabolism and the range of other functions of the alarmone may greatly vary across species [32, 60, 61]. While it has thus been well-established that regulation by ppGpp is an evolutionary conserved mechanism of growth control in the bacterial cell, our analysis provides a new perspective by suggesting that ppGpp enables optimal reallocation of resources after a growth transition, dynamically maximizing the accumulation of biomass.

The model on which the above results are based is built from first principles by distinguishing two fundamental cellular processes: metabolism (converting nutrients to precursors) and gene expression (converting precursors to the proteins that make up biomass) (Fig. 2.1). Despite its simplicity, our self-replicator model is capable of reproducing the empirical growth laws and of making testable predictions on the time-course profile of the resource allocation variable α and on the concentrations p and r of components of the gene expression machinery and metabolic machinery, respectively (see Fig. 2.8 and below). The model can be easily extended with more details on protein synthesis, central carbon and energy metabolism, stress systems, or cell membranes, but this would make the mathematical analysis of the model dynamics and the optimal control problem more complicated. Notice, however, that the direct numerical approach for solving the optimal control problem remains applicable, even for more fine-grained models (Fig. 2.4, see also [27]).

The comparison of different control strategies during a classical growth transition should be interpreted carefully, in a qualitative rather than quantitative manner. Whereas the differences in performance based on the biomass ratio $\mathtt{Vol}/\mathtt{Vol}_{opt}$ of the control strategies are robust, the absolute numbers for the biomass ratio will depend on details of the growth experiment chosen and the exact parameter values. Another implicit assumption in the analysis of the control strategies is that the costs of their molecular implementation can be neglected. This is not true in general, since every control strategy requires resources to be diverted towards the synthesis of sensory systems and regula-

tory proteins, with possibly detrimental effects on growth. In other words, a control strategy entails a trade-off between the growth burden of regulation and the growth benefit of the improved capability to adapt to changes in the environment [62, 63]. The analysis of control strategies could be refined by adding a reaction to the self-replicator that models the loss of resources incurred by regulatory strategies. While in general the growth burden of a control strategy requiring information on several aspects of cellular physiology is expected to be higher, notice that a single regulatory system may be capable of sensing more than one variable. For example, we show that ppGpp levels in the cell carry information on both the metabolic and the gene expression state (Fig. 2.8), thus integrating several signals in a cost-efficient manner.

The model predictions for the dynamical adaptation of resource allocation after a nutrient upshift suggest several interesting experimental tests. In particular, the switching profile of the resource allocation variable α is a promising candidate for experimental validation. The most straightforward option would be direct measurement of the synthesis rate of ribosomal proteins, using a translational fusion of a fluorescent reporter with a ribosomal protein [45, 64]. However, a more indirect approach based on the quantification of ppGpp concentrations in the cell or the activity of the ribosomal RNA (rRNA) promoters would also be a possibility. Interestingly, some data are already available in the literature. For instance, Gausing has reviewed data on the synthesis of ribosomal proteins after a nutrient upshift, showing that the synthesis rate goes through "a series of rapid changes" resembling oscillations [65]. Later work attributed this pattern to regulation on the transcriptional level [66]. Friesen *et al.* observed oscillatory patterns in ppGpp concentrations after a nutrient upshift, with an initial response resembling bang control for an upshift to a particularly rich medium [67]. Murray *et al.* also present data on the ppGpp concentration after a nutrient upshift [49], but with a lower temporal resolution and no clear oscillatory pattern. All of the above measurements were carried out on the population level, which means that switching patterns may be obscured by desynchronisation of the individual cells. More sophisticated experimental set-ups are necessary for the decisive validation of the model predictions, allowing gene expression in single cells to be followed over time in tightly regulated growth conditions [68, 69]. In addition, the model could be validated on other dynamical scenarios, for example nutrient downshifts [49, 70].

Apart from its interest for fundamental science, resource allocation is also a critical question in biotechnology, where there exists an inherent trade-off between the maximization of yield and productivity [71]. High yield means that most of the substrate is converted to a metabolite, peptide or recombi-

nant protein of interest, but this leads to low productivity if the remaining nutrient influx is insufficient to sustain population growth. Engineered control of resource allocation may help in establishing the right trade-off, the most profitable balance between yield and productivity, in a biotechnological process. Such a trade-off could be attained either in steady-state conditions (the incoming nutrient flux is optimally distributed over growth and production) or in dynamical conditions (alternating utilization of the incoming nutrient flux for growth or production) [72–74]. When extended with heterologous metabolic pathways, the self-replicator models used in this study would provide an adequate *in-silico* test bed for the rapid screening and comparison of alternative control strategies in bioprocess engineering.

2.11 Methods

2.11.1 Steady-state analysis of model

The nondimensional version of the model, given by Eqs 2.11-2.12, was used for a steady-state analysis of the self-replicator. Eqs 2.11-2.12 were derived from the original model of Eqs 2.3-2.4 by means of the following rescalings:

$$\hat{p} = \beta\, p, \quad \hat{r} = \beta\, r, \quad \hat{t} = k_R\, t, \quad E_M = e_M/k_R, \quad K = \beta K_R.$$

As shown in S1 Text, for a constant environment E_M and constant resource allocation α, the system has two steady states: a trivial unstable steady state $(\hat{p}^*, \hat{r}^*) = (0, 1)$, allowing no growth in the absence of precursors, and a steady state with a positive growth rate given by

$$(\hat{p}^*, \hat{r}^*) = \left(\frac{(1-\alpha)\, E_M - \alpha + \sqrt{[(1-\alpha)\, E_M - \alpha]^2 + 4\alpha\,(1-\alpha)\, E_M\, K}}{2\alpha}, \alpha \right). \tag{2.21}$$

The two eigenvalues of the Jacobian matrix evaluated at $(\hat{p}^*, \hat{r}^*)$ are negative (S1 Text), so that this steady state is stable.

The growth rate at steady state, as a function of $\hat{p}^*$ and $\hat{r}^*$, is given by Eq. 2.13, which we repeat here for clarity:

$$\hat{\mu}^* = \frac{\hat{p}^*}{K + \hat{p}^*}\, \hat{r}^*.$$

Evaluating $d\hat{p}/dt = 0$ at $(\hat{p}^*, \hat{r}^*)$ allows $\hat{r}^*$, and therefore $\hat{\mu}^*$, to be written as a function of $\hat{p}^*$ (S1 Text). Accordingly, we can compute $\partial\hat{\mu}^*/\partial\hat{p}^*$ and, when

setting this partial derivative to 0, determine the maximum growth rate at steady state μ^*_{opt} and the optimal resource allocation α^*_{opt} bringing about this maximal growth rate. As shown in S1 Text, μ^*_{opt} and α^*_{opt} can be written as explicit functions of either the environment E_M:

$$\alpha^*_{opt} = \frac{E_M + \sqrt{K\,E_M}}{E_M + 2\sqrt{K\,E_M} + 1}, \qquad \hat{\mu}^*_{opt} = \frac{E_M}{E_M + 2\sqrt{K\,E_M} + 1}, \quad (2.22)$$

or the precursor abundance $\hat{p}^*_{opt}$:

$$\alpha^*_{opt} = \frac{\hat{p}^*_{opt}}{\hat{p}^*_{opt} + \frac{K}{K+\hat{p}^*_{opt}}(1+\hat{p}^*_{opt})}, \qquad \hat{\mu}^*_{opt} = \frac{\hat{p}^{*2}_{opt}}{\hat{p}^{*2}_{opt} + 2K\hat{p}^*_{opt} + K}. \quad (2.23)$$

The above equations were used for the derivation of the control strategies (see below).

2.11.2 Model fitting

As can be seen by comparing Figs 2.3*A* and 2.3*B*, growth-rate maximization in the self-replicator model leads to a good qualitative correspondence with the growth laws. In order to determine if a good quantitative fit of the model with the data from Scott *et al.* [12] can be obtained, for reasonable parameter values, we estimated e_M and k_R in Eqs 2.3-2.4 from the measured RNA/protein mass ratios. At steady state, the RNA/protein mass ratio can be interpreted as proportional to $\hat{r}^*$ (and thus α^*_{opt}), with an unknown (dimensionless) proportionality constant γ (see [12] for details on the use of the RNA/protein mass ratio as a proxy for the ribosomal protein mass fraction):

$$\hat{r}^* = \alpha^*_{opt} = \gamma\,\frac{\text{RNA mass}}{\text{protein mass}}. \quad (2.24)$$

Reformulating Eq. 2.22 in terms of the original parameters e_M and k_R, which have physical dimensions facilitating the biological interpretation of their values, we obtain a straighforward relation between e_M, k_R, K, α^*_{opt} and μ^*_{opt}:

$$\alpha^*_{opt} = \frac{e_M + \sqrt{K\,e_M\,k_R}}{e_M + 2\sqrt{K\,e_M\,k_R} + k_R}, \qquad \mu^*_{opt} = \frac{e_M\,k_R}{e_M + 2\sqrt{K\,e_M\,k_R} + k_R}. \quad (2.25)$$

Eqs 2.24-2.25 were used to estimate values of k_R and γ, as well as e_M for each of the six growth conditions, from the measurements of the growth rate and the RNA/protein mass ratio. The value K was not estimated from the

experimental data, but set to a value inferred from the literature (S1 Text). The optimization process was carried out by means of the differential evolution algorithm of Storn and Price [75]. The results are shown in Fig. 2.3*B*, while the estimated parameter values are summarized in S1 Table. The parameter values are in very good agreement with order-of-magnitude values determined from the literature (S2 Text and S1 Table).

2.11.3 Solution of optimal control problem

The optimal control problem of Eq. 2.10 consists in identifying the function $\alpha_{opt}(t)$ that maximizes the integral of the growth rate $\hat{\mu}$ over an interval $[0, \tau]$. In order to solve this problem, we first redefined it over an infinite horizon (*i.e.*, $\tau \to \infty$) in order to avoid boundary effects occurring over finite time intervals, in particular the depletion of precursors just before reaching τ. With $\mathcal{U} = \{\alpha : \mathbb{R}^+ \to [0, 1]\}$ the set of admissible controls, the full optimization problem for the nondimensionalized system is given by

$$\max_{\alpha \in \mathcal{U}} J(\alpha) \equiv \int_0^\infty \hat{r}(\hat{t}) \, \frac{\hat{p}(\hat{t})}{K + \hat{p}(\hat{t})} \, d\hat{t}. \tag{2.26}$$

Since $J(\alpha)$ diverges, we actually consider overtaking optimality: A solution is overtaking optimal if its performance index catches up with the performance index of any other solution ([40], see S3 Text for details).

Necessary conditions on optimal trajectories can be obtained by the Infinite Horizon Maximum Principle [40], an extension of the well-known Pontryagin Maximum Principle. Analysis of the Hamiltonian of the system of Eqs 2.11-2.12 and the associated adjoint system shows that the optimal trajectory is a concatenation of bang arcs ($\alpha(\cdot) = 0$ or $\alpha(\cdot) = 1$) and possibly a singular arc corresponding to the optimal steady state $(\hat{p}(t), \hat{r}(t)) = (\hat{p}^*_{opt}, \hat{r}^*_{opt})$, that is, the steady state leading to the optimal growth rate $\hat{\mu}^*_{opt}$ in the new environment after the upshift (S3 Text). Moreover, from the Kelley condition [76], we can show that if the optimal trajectory has a singular arc, then it must enter this singular arc *via* a chattering arc, *i.e.*, with an infinite number of switches of $\alpha(\cdot)$ between 0 and 1 (S3 Text). The chattering arc is characterized by a switching curve $\hat{r} = \varphi(\hat{p})$ in the $(\hat{p}, \hat{r})$-plane, which passes through $(\hat{p}^*_{opt}, \hat{r}^*_{opt})$. The switching curve divides the phase plane into two regions, such that $\alpha(t)$ switches to 0 when the system is in the region above φ and to 1 when the system is below φ (S3 Text and Fig. 2.4).

The above results have led to the conjectured optimal solution of Eq. 2.14. In parallel, we numerically solved the problem of Eq. 2.26 by a direct method using the `bocop` software [41]. A time discretization allows the optimal control problem to be transformed into a nonlinear optimization problem, solved

here by interior point techniques. A discretization by a Lobatto IIIC formula (6th order) was used with 4000 time steps, and the relative tolerance for the NLP solver was set to 10^{-14}. The optimal trajectories thus obtained are composed of a chattering arc followed by a steady state corresponding to the singular arc (Fig. 2.4). The switching curve $\varphi(\hat{p})$ was computed from numerical simulations with different initial conditions.

2.11.4 Specification and analysis of control strategies

As described in the *Results* section, we are interested in control strategies satisfying the following conditions:

(C1) The control laws are static functions of the system variables (as opposed to, for instance, functions that depend on derivatives or integrals of the variables).

(C2) For any given constant environment E_M, they drive the self-replicator system towards a unique stable steady state that is not trivial, *i.e.*, with nonzero growth rate.

(C3) This steady state corresponds to the optimal steady state $(\hat{p}^*_{opt}, \hat{r}^*_{opt})$, allowing growth at the maximal rate μ^*_{opt}.

It can be directly verified from the functions f, g, and h defining the nutrient-only, precursor-only, and on-off control strategies (Eqs 2.15, 2.17, and 2.19) that they are indeed static functions of the system variables (or the system input, in the case of the nutrient-only strategy). Here we show that the other two conditions are also satisfied for all three strategies.

Following Eq. 2.15, the nutrient-only strategy is defined by $\alpha = f(E_M)$, so that α is constant after the upshift. As shown above and in S1 Text, this means that the system controlled by the nutrient-only strategy has a single nontrivial stable steady state (Condition C2). In addition, in this case the optimal steady state is attained for α^*_{opt} defined as in Eq. 2.22, and the following function f therefore guarantees Condition C3:

$$f(E_M) = \frac{E_M + \sqrt{K E_M}}{E_M + 2\sqrt{K\, E_M} + 1}. \tag{2.27}$$

In S1 Text, it is shown that Eq. 2.27 is the only definition of f satisfying all conditions. S1 Figure shows a plot of $f(E_M)$ together with a biologically plausible Michaelis-Menten approximation (Eq. 2.16).

The full specification of the precursor-only strategy demands an expression for the function g in Eq. 2.17. Recall that Eq. 2.23 defines α^*_{opt} in terms

of the precursor concentration $\hat{p}^*_{opt}$, which leads us to propose the following function g:

$$g(\hat{p}) = \frac{\hat{p}}{\hat{p} + \frac{K}{K+\hat{p}}(1+\hat{p})}. \tag{2.28}$$

As shown in S1 Text by computing the Jacobian, the system given by Eqs 2.11-2.12 and 2.28 has a single nontrivial stable steady state for any environment E_M (Condition C2). Moreover, Eq. 2.28 guarantees this steady state to be optimal (Condition C3). This can be seen by noting that at steady state, $d\hat{r}/dt = 0$ implies $\hat{r}^* = g(\hat{p}^*)$ (Eq. 2.12). In order for the self-replicator to attain a maximal growth rate at steady rate, Eq. 2.23 needs to be satified, which is the case for the above choice of the function g. Like for f, Eq. 2.28 is the only choice for g satisfying C1-C3. S1 Figure shows a plot of $g(\hat{p})$ together with a biologically plausible Hill approximation (Eq. 2.18).

The on-off control strategy is defined in Eq. 2.19 and repeated below:

$$h(\hat{p},\hat{r}) = \begin{cases} 0, \text{ if } \hat{r} > g(\hat{p}), \\ 1, \text{ if } \hat{r} < g(\hat{p}), \\ \alpha^*_{opt}, \text{ if } (\hat{p},\hat{r}) = (\hat{p}^*_{opt}, \hat{r}^*_{opt}). \end{cases} \tag{2.29}$$

This strategy drives the system to a single steady state, because the $\hat{p}$-nullcline crosses the function $g(\hat{p})$ only once, as shown graphically in Fig. 2.7*A*. In S1 Text we argue that this steady state is stable, by taking into account so-called sliding modes on the switching curve [77] (Condition C2). Moreover, the steady state coincides with the optimal steady state $(\hat{p}^*_{opt}, \hat{r}^*_{opt})$ by construction, so that Condition C3 is satisfied as well. Fig 2.8*A* shows a plot of $h(\hat{p},\hat{r})$.

Note that since $h(\cdot)$ is discontinuous, numerical instabilities occur during simulations. We therefore used the following continuous approximation of this function:

$$\frac{g(\hat{p})^{100}}{g(\hat{p})^{100} + \hat{r}^{100}}, \text{ if } \hat{r} \neq g(\hat{p}). \tag{2.30}$$

The approximation causes α to take intermediate values (instead of 0 or 1) just before reaching the optimal steady state in Fig 2.7*C*. For numerical simulations of the ODE system, we used the CVODE solver [78] from SUNDIALS 2.6.2 [79].

2.12 S1 Text – Model derivation and analysis

2.12.1 Model formulation

The time evolution of the total mass of each component of the self-replicator can be written as follows:

$$\begin{aligned} \frac{dP}{dt} &= V_M(t) - V_R(t), \\ \frac{dM}{dt} &= (1-\alpha(t))\, V_R(t), \\ \frac{dR}{dt} &= \alpha(t)\, V_R(t), \end{aligned} \tag{2.31}$$

where P, M, R [g] denote the total mass of precursors, metabolic machinery and gene expression machinery, respectively. V_M [g h^{-1}] is the rate of production of precursors by metabolism and V_R [g h^{-1}] the rate of utilisation of precursors for gene expression.

Dividing the mass variables by the total time-varying volume $\texttt{Vol}(t)$ of the system, we obtain the concentration variables $p = P/\texttt{Vol}$, $m = M/\texttt{Vol}$, $r = R/\texttt{Vol}$ [g L^{-1}]. The dynamics of the concentration variables then follows with Eq. 2.31:

$$\begin{aligned} \frac{dp}{dt} &= \frac{V_M(t)}{\texttt{Vol}} - \frac{V_R(t)}{\texttt{Vol}} - \frac{1}{\texttt{Vol}}\frac{d\texttt{Vol}}{dt}\, p, \\ \frac{dm}{dt} &= (1-\alpha(t))\frac{V_R(t)}{\texttt{Vol}} - \frac{1}{\texttt{Vol}}\frac{d\texttt{Vol}}{dt}\, m, \\ \frac{dr}{dt} &= \alpha(t)\,\frac{V_R(t)}{\texttt{Vol}} - \frac{1}{\texttt{Vol}}\frac{d\texttt{Vol}}{dt}\, r. \end{aligned} \tag{2.32}$$

At this point, we define $v_M = V_M/\texttt{Vol}$ and $v_R = V_R/\texttt{Vol}$ [g L^{-1} h^{-1}] as the mass fluxes per unit volume. Moreover, with the definition of the volume in terms of the total protein mass in Eq. 2.2 of the main text, that is, $\texttt{Vol} = \beta\,(M+R)$, we find that

$$\frac{1}{\texttt{Vol}}\frac{d\texttt{Vol}}{dt} = \frac{\beta}{\texttt{Vol}}\frac{d(M+R)}{dt} = \beta\,\frac{V_R(t)}{\texttt{Vol}} = \beta\, v_R(t). \tag{2.33}$$

This leads to the system

$$\frac{dp}{dt} = v_M(t) - v_R(t)\,(1+\beta\, p), \tag{2.34}$$

$$\frac{dr}{dt} = v_R(t)\,(\alpha(t) - \beta\, r), \tag{2.35}$$

where the equation for $m(t)$ is omitted since by construction $r(t)+m(t) = 1/\beta$ and $dr/dt + dm/dt = 0$.

As stated in the main text, we use Michaelis-Menten kinetics to express v_M and v_R in terms of the system variables:

$$\begin{aligned} v_M(t) &= m(t)\, k_M\, \frac{s(t)}{K_M + s(t)} = \left(\frac{1}{\beta} - r(t)\right)\, e_M(t), \\ v_R(t) &= r(t)\, k_R\, \frac{p(t)}{K_R + p(t)}, \end{aligned}$$

with rate constants k_M, k_R [h^{-1}] and half-saturation constants K_M, K_R [g L^{-1}]. $s(t)$ is an exogenous variable representing the nutrient concentration in the external medium. We simplify $v_M(t)$ by defining the environmental input $e_M(t) = k_M\, s(t)/(K_M + s(t))$. Throughout the paper, as explained in the main text, we assume the environment is constant, *i.e.*, $e_M(t) = e_M$.

Finally, the growth rate μ [h^{-1}] is defined as the relative increase of the volume of the self-replicator. From Eq. 2.33, it follows that:

$$\mu(t) = \frac{1}{\mathtt{Vol}}\frac{d\mathtt{Vol}}{dt} = \beta\, v_R(t). \tag{2.36}$$

2.12.2 Nondimensionalization of the system

For the sake of simplifying the proofs and derivations below, we define the following nondimensional variables:

$$\hat{p} = \beta\, p, \quad \hat{r} = \beta\, r, \quad \hat{t} = k_R\, t.$$

When injecting these into Eq. 2.34, we obtain

$$\frac{k_R}{\beta}\,\frac{d\hat{p}}{d\hat{t}} = \left(\frac{1}{\beta} - \frac{\hat{r}}{\beta}\right)\, e_M - \frac{\hat{r}}{\beta}\, k_R\, \frac{\hat{p}}{\beta K_R + \hat{p}}\,(1+\hat{p}),$$

which simplifies to

$$\frac{d\hat{p}}{d\hat{t}} = (1-\hat{r})\,\frac{e_M}{k_R} - \hat{r}\,\frac{\hat{p}}{\beta K_R + \hat{p}}\,(1+\hat{p}).$$

In a similar manner, we derive the time evolution of the nondimensional $\hat{r}$, and thus obtain the system

$$\begin{aligned} \frac{d\hat{p}}{d\hat{t}} &= (1-\hat{r})\, E_M - (1+\hat{p})\,\frac{\hat{p}}{K+\hat{p}}\,\hat{r}, \\ \frac{d\hat{r}}{d\hat{t}} &= (\alpha - \hat{r})\,\frac{\hat{p}}{K+\hat{p}}\,\hat{r}, \end{aligned} \tag{2.37}$$

with the lumped parameters $E_M = e_M/k_R$ and $K = \beta\, K_R$. The corresponding nondimensionalized growth rate is given by

$$\hat{\mu} = \frac{\mu}{k_R} = \frac{\hat{p}}{K + \hat{p}}\, \hat{r}. \tag{2.38}$$

2.12.3 Steady-state growth of the self-replicator

If we suppose $E_M > 0$, $K > 0$ and $\alpha \in]0, 1[$, there is a trivial unstable steady state at $(0, 1)$. A second steady-state exists for the point in which $\hat{r}^* = \alpha$ and $\hat{p}^*$ is a root of the following polynomial:

$$\alpha\, \hat{p}^2 + (\alpha - (1 - \alpha)\, E_M)\, \hat{p} - (1 - \alpha)\, E_M\, K.$$

If we keep the only admissible root for this polynomial (*i.e.*, for which $\hat{p} \geq 0$), the second steady state is given by

$$(\hat{p}^*, \hat{r}^*) = \left(\frac{(1 - \alpha)\, E_M - \alpha + \sqrt{[(1 - \alpha)\, E_M - \alpha]^2 + 4\alpha\, (1 - \alpha)\, E_M\, K}}{2\alpha}, \alpha \right). \tag{2.39}$$

We can determine the stability of this steady state by looking at the Jacobian matrix J of the ODE system:

$$J = \begin{pmatrix} -\frac{\hat{r}}{K+\hat{p}} \left[\hat{p} + (1 + \hat{p})\, \frac{K}{K+\hat{p}} \right] & -E_M - (1 + \hat{p}) \frac{\hat{p}}{K+\hat{p}} \\ (\alpha - \hat{r})\, \hat{r}\, \frac{K}{(K+\hat{p})^2} & (\alpha - 2\hat{r})\, \frac{\hat{p}}{K+\hat{p}} \end{pmatrix}. \tag{2.40}$$

Evaluated at the point $(\hat{p}^*, \hat{r}^*)$, the Jacobian matrix becomes

$$J_{(\hat{p}^*, \hat{r}^*)} = \begin{pmatrix} -\frac{\alpha}{K+\hat{p}^*} \left[\hat{p}^* + (1 + \hat{p}^*) \frac{K}{K+\hat{p}^*} \right] & -E_M - (1 + \hat{p}^*) \frac{\hat{p}^*}{K+\hat{p}^*} \\ 0 & -\alpha \frac{\hat{p}^*}{K+\hat{p}^*} \end{pmatrix}.$$

Since $\hat{p}^*$, α, E_M, $K > 0$, the two eigenvalues are negative and therefore the steady state $(\hat{p}^*, \hat{r}^*)$ is stable (see also the streamlines in Figure 2.2*A* in the main text). It means that for fixed environmental conditions E_M and resource allocation α, the self-replicator converges towards a steady state in which the concentration variables are constant.

One can now easily derive the steady-state growth rate, denoted $\hat{\mu}^*$. By substituting Eq. 2.38 into the first ODE of the system of Eq. 2.37, we find at steady state:

$$\left(\frac{d\hat{p}}{d\hat{t}} \right)_{(\hat{p}^*, \hat{r}^*)} = 0 = (1 - \alpha)\, E_M - (1 + \hat{p}^*)\, \hat{\mu}^*,$$

which by means of Eq. 2.39 gives the following relation:

$$\hat{\mu}^* = \frac{(1-\alpha)\,E_M}{1+\hat{p}^*} = \frac{2\alpha(1-\alpha)\,E_M}{(1-\alpha)\,E_M + \alpha + \sqrt{\left[(1-\alpha)\,E_M - \alpha\right]^2 + 4\alpha(1-\alpha)\,E_M\,K}}. \tag{2.41}$$

Finally, we can transform this expression to obtain

$$\hat{\mu}^* = \begin{cases} \frac{(1-\alpha)\,E_M+\alpha-\sqrt{\left[(1-\alpha)\,E_M-\alpha\right]^2+4(1-\alpha)\,\alpha\,E_M\,K}}{2(1-K)} & \text{for } K \neq 1, \\ \frac{\alpha\,(1-\alpha)\,E_M}{\alpha+(1-\alpha)\,E_M} & \text{for } K = 1. \end{cases} \tag{2.42}$$

This function of α is plotted in Figure 2.2B in the main text.

2.12.4 Maximization of growth rate at steady state

We are interested in the steady state at which growth occurs at the maximum rate. The growth rate at steady state $\hat{\mu}^*$ is given by

$$\hat{\mu}^* = \frac{\hat{p}^*}{K+\hat{p}^*}\,\hat{r}^*. \tag{2.43}$$

From the first ODE of the system of Eq. 2.37, we have

$$\hat{r}^* = \frac{E_M}{E_M + \frac{\hat{p}^*}{K+\hat{p}^*}(1+\hat{p}^*)}. \tag{2.44}$$

Substituting Eq. 2.44 into Eq. 2.43, we obtain

$$\hat{\mu}^* = \frac{E_M\,\hat{p}^*}{\hat{p}^{*2} + (E_M+1)\,\hat{p}^* + E_M\,K}. \tag{2.45}$$

The value of $\hat{p}^*$ maximizing $\hat{\mu}^*$ can be determined from

$$\frac{\partial\hat{\mu}^*}{\partial\hat{p}^*} = \frac{E_M\,(E_M\,K - \hat{p}^{*2})}{\left(\hat{p}^{*2} + (E_M+1)\,\hat{p}^* + E_M\,K\right)^2}, \tag{2.46}$$

by looking at the values of $\hat{p}^*$ for which this derivative equals 0. It follows that $\hat{\mu}^*$ is maximal for

$$\hat{p}^* = \hat{p}^*_{opt} = \sqrt{K\,E_M}. \tag{2.47}$$

By substituting $\hat{p}^*_{opt}$ and α^*_{opt} for $\hat{p}^*$ and $\hat{r}^*$, respectively, in Eq. 2.44, we obtain the resource allocation maximizing the growth rate

$$\alpha^*_{opt} = \frac{E_M + \sqrt{K\,E_M}}{E_M + 2\sqrt{K\,E_M} + 1}. \tag{2.48}$$

Finally, injecting this result into Eq. 2.43 we obtain the optimal steady-state growth rate:

$$\hat{\mu}^*_{opt} = \frac{E_M}{E_M + 2\sqrt{K\,E_M} + 1}. \tag{2.49}$$

In addition, by using Eq. 2.47, we can write α^*_{opt} and $\hat{\mu}^*_{opt}$ as a function of $\hat{p}^*_{opt}$ only:

$$\alpha^*_{opt} = \frac{\hat{p}^*_{opt}}{\hat{p}^*_{opt} + \frac{K}{K+\hat{p}^*_{opt}}(1+\hat{p}^*_{opt})}, \qquad \hat{\mu}^*_{opt} = \frac{\hat{p}^{*2}_{opt}}{\hat{p}^{*2}_{opt} + 2K\hat{p}^*_{opt} + K}. \tag{2.50}$$

2.12.5 Analysis of the control strategies

In this section, we derive the main results for the functions f, g, and h defining the nutrient-only, precursor-only, and on-off control strategies. For each of these, we prove that the Conditions C1, C2 and C3 from the *Methods* section are satisfied, which we repeat here for clarity:

(C1) The control laws are static functions of the system variables (as opposed to, for instance, functions that depend on derivatives or integrals of the variables).

(C2) For any given constant environment E_M, they drive the self-replicator system towards a unique stable steady state that is not trivial, *i.e.*, with nonzero growth rate.

(C3) This steady state corresponds to the optimal steady state $(\hat{p}^*_{opt}, \hat{r}^*_{opt})$, allowing growth at the maximal rate μ^*_{opt}.

Nutrient-only strategy

The nutrient-only strategy is defined by:

$$\alpha = f(E_M) = \frac{E_M + \sqrt{K E_M}}{E_M + 2\sqrt{K\,E_M} + 1}. \tag{2.51}$$

It drives the system to the optimal steady state by measuring the environment E_M. Note that Condition C1 is satisfied by definition.

By injecting Eq. 2.51 into Eq. 2.37, the ODE system under the control of f becomes:

$$\begin{aligned} \frac{d\hat{p}}{d\hat{t}} &= (1-\hat{r})\,E_M - (1+\hat{p})\,\frac{\hat{p}}{K+\hat{p}}\,\hat{r}, \\ \frac{d\hat{r}}{d\hat{t}} &= (f(E_M)-\hat{r})\,\frac{\hat{p}}{K+\hat{p}}\,\hat{r}. \end{aligned} \tag{2.52}$$

Since E_M is constant on the interval of interest (starting right after the upshift), we are in the case of Section 2.12.3 (*i.e.*, α constant). In particular, the system has two steady states: a trivial unstable one at (0, 1) (with zero growth), and a stable one defined by Eq. 2.39 (Condition C2). Since $f(E_M) = \alpha^*_{opt}$, we conclude from the derivations in Section 2.12.4 that the stable steady state is optimal for every environment E_M (Condition C3).

It is interesting to note that the expression in Eq. 2.51 is the only function $f(E_M)$ satisfying C1-C3. We can prove this statement by contradiction. Assume a control strategy $c(E_M)$ satisfying C1-C3, and different from $f(E_M)$, *i.e.*, there exists $E_M = E_{M1}$ such that $c(E_{M1}) \neq f(E_{M1})$. In this environment, the system reaches a steady state $(\hat{p}^*_1, \hat{r}^*_1)$ with $\hat{r}^*_1 = c(E_{M1}) \neq f(E_{M1})$. However, by Eq. 2.48 the optimal value for $\hat{r}^*$ in this environment is given by $f(E_{M1})$. So, the control law $c(E_M)$ does not drive the system to the optimal steady state in this environment, in contradiction with Condition C3.

2.12.6 Precursor-only strategy

The precursor-only strategy is defined by:

$$\alpha = g(\hat{p}) = \frac{\hat{p}}{\hat{p} + \frac{K}{K+\hat{p}}(1+\hat{p})}. \tag{2.53}$$

Here as well, C1 is satisfied by construction.

The ODE system under the control of g becomes

$$\begin{aligned} \frac{d\hat{p}}{d\hat{t}} &= (1-\hat{r})\, E_M - (1+\hat{p})\, \frac{\hat{p}}{K+\hat{p}}\, \hat{r}, \\ \frac{d\hat{r}}{d\hat{t}} &= (g(\hat{p}) - \hat{r})\, \frac{\hat{p}}{K+\hat{p}}\, \hat{r}. \end{aligned} \tag{2.54}$$

The nullcline for $\hat{p}$ remains unchanged and is defined by

$$\frac{d\hat{p}}{dt} = 0 \Leftrightarrow \hat{r} = \frac{E_M}{E_M + \frac{\hat{p}}{K+\hat{p}}(1+\hat{p})}, \tag{2.55}$$

while the nullcline for $\hat{r}$ is

$$\frac{d\hat{r}}{dt} = 0 \Leftrightarrow \begin{cases} \hat{p} = 0, \\ \hat{r} = 0, \\ \hat{r} = \frac{\hat{p}}{\hat{p} + \frac{K}{K+\hat{p}}(1+\hat{p})}. \end{cases} \tag{2.56}$$

Hence, we also have a trivial unstable steady state at (0,1) (with zero growth). The second steady state is obtained from Eqs 2.55-2.56:

$$\frac{E_M}{E_M + \frac{\hat{p}^*}{K+\hat{p}^*}(1+\hat{p}^*)} = \frac{\hat{p}^*}{\hat{p}^* + \frac{K}{K+\hat{p}^*}(1+\hat{p}^*)},$$

which we rearrange into

$$\hat{p}^* E_M + \frac{K}{K+\hat{p}^*}(1+\hat{p}^*)E_M = \hat{p}^* E_M + \frac{\hat{p}^*}{K+\hat{p}^*}(1+\hat{p}^*)\hat{p}^*.$$

This leads to

$$\hat{p}^* = \sqrt{KE_M},$$

and therefore

$$\hat{r}^* = g(\hat{p}^*) = \frac{\sqrt{KE_M}}{\sqrt{KE_M} + \frac{K}{K+\sqrt{KE_M}}(1+\sqrt{KE_M})} = \frac{E_M + \sqrt{KE_M}}{E_M + 2\sqrt{KE_M} + 1}.$$

From Eqs 2.47-2.48, we recognize the optimal steady state for the environment E_M, validating Condition C3. We now look for the stability of this (optimal) steady state by deriving the Jacobian of this system:

$$J = \begin{pmatrix} -\frac{\hat{r}}{K+\hat{p}}\frac{\hat{p}^2+2K\hat{p}+K}{\hat{p}+K} & -E_M - \frac{\hat{p}}{K+\hat{p}}(1+\hat{p}) \\ \frac{\hat{r}}{K+\hat{p}}\left[\frac{K}{K+\hat{p}}(g(\hat{p})-\hat{r}) + \hat{p}K\frac{\hat{p}^2+2\hat{p}+K}{(\hat{p}^2+2K\hat{p}+K)^2}\right] & \frac{\hat{p}}{K+\hat{p}}(g(\hat{p})-2\hat{r}) \end{pmatrix}. \tag{2.57}$$

Evaluated at $(\hat{p}^*, \hat{r}^*) = (\sqrt{KE_M}, g(\sqrt{KE_M}))$, the Jacobian becomes

$$J_{(\hat{p}^*,\hat{r}^*)} = \begin{pmatrix} -\frac{\sqrt{E_M}}{\sqrt{K}+\sqrt{E_M}} & -E_M - \frac{\sqrt{E_M}}{\sqrt{K}+\sqrt{E_M}}(1+\sqrt{KE_M}) \\ \frac{\sqrt{E_M}}{\sqrt{K}+\sqrt{E_M}}\frac{KE_M+2\sqrt{KE_M}+K}{K(E_M+2\sqrt{KE_M}+1)^2}g(\sqrt{KE_M}) & -\frac{\sqrt{E_M}}{\sqrt{K}+\sqrt{E_M}}g(\sqrt{KE_M}) \end{pmatrix}. \tag{2.58}$$

Since K, E_M, and $g(\sqrt{KE_M}) > 0$, it follows immediately that the real part of the eigenvalues of this matrix are both negative.[1] Hence, the non-trivial steady state is stable, completing the proof of Condition C2.

Here again, it is interesting to observe that the expression in Eq. 2.53 is the only function $g(\hat{p})$ satisfying C1-C3. This can be proven in a similar way as for f.

1. Notice that the eigenvalues λ_1 and λ_2 of $J_{(\hat{p}^*,\hat{r}^*)}$ satisfy the inequalities $\mathrm{Tr}(J) = \lambda_1 + \lambda_2 < 0$ and $\det(J) = \lambda_1\lambda_2 > 0$.

2.12.7 On-off strategy

The on-off strategy is defined by:

$$\alpha = h(\hat{p}, \hat{r}) = \begin{cases} 0, \text{ if } \hat{r} > g(\hat{p}), \\ 1, \text{ if } \hat{r} < g(\hat{p}), \\ \alpha^*_{opt}, \text{ if } (\hat{p}, \hat{r}) = (\hat{p}^*_{opt}, \hat{r}^*_{opt}). \end{cases} \tag{2.59}$$

h is a static function of $\hat{p}$ and $\hat{r}$ (Condition C1).

As a consequence, the ODE system under the control of h is given by

$$\begin{aligned} \frac{d\hat{p}}{d\hat{t}} &= (1 - \hat{r})\, E_M - (1 + \hat{p})\, \frac{\hat{p}}{K + \hat{p}}\, \hat{r}, \\ \frac{d\hat{r}}{d\hat{t}} &= (h(\hat{p}, \hat{r}) - \hat{r})\, \frac{\hat{p}}{K + \hat{p}}\, \hat{r}. \end{aligned} \tag{2.60}$$

Notice that the system has a discontinuitous right-hand side, due to the fact that α switches between 0 and 1 on $\hat{r} = g(\hat{p})$. Fig. 2.9 shows the dynamics of the system in the phase plane. Due to the direction of the vector fields relative to $\hat{r} = g(\hat{p})$, a *sliding mode* occurs on the latter curve [77]. The system is seen to evolve towards a locally asymptotically stable steady state, which is the single non-trivial steady state (Condition C2). This steady state coincides with the intersection of $\hat{r} = g(\hat{p})$ and the $\hat{p}$-nullcline, which is the steady state $(\hat{p}^*_{opt}, \hat{r}^*_{opt})$ allowing maximal growth, thus verifying Condition C3.

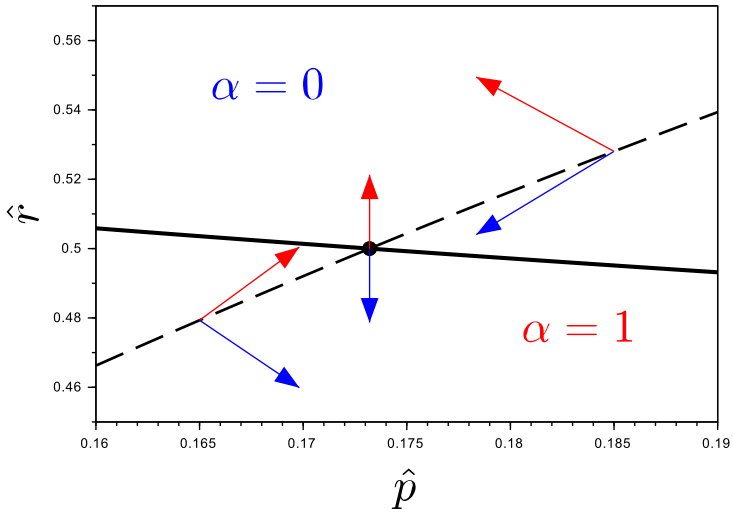

Figure 2.9 – **Local stability of the on-off strategy.** The on-off strategy sets α to a value of 0 (1) when $\hat{r} > g(\hat{p})$ ($\hat{r} < g(\hat{p})$). The solid, black curve is the $\hat{p}$-nullcline. The dashed, black curve is the curve $\hat{r} = g(\hat{p})$. The arrows represent the vector fields for $\alpha = 0$ (in blue) and $\alpha = 1$ (in red). The intersection of the $\hat{p}$-nullcline and the curve $\hat{r} = g(\hat{p})$ corresponds to a unique non-trivial stable steady state, which is equal to $(\hat{p}^*_{opt}, \hat{r}^*_{opt})$ by Eq. 2.60.

2.13 S2 Text – Model parameters

Most of the conclusions of this paper are parameter-independent in the range of physically admissible values. The exact parameter values used in the simulations aim to represent relevant orders of magnitude. They were derived from the available literature on fast-growing bacteria (mostly *Escherichia coli*). This document describes this derivation for each parameter. In the *Methods* section of the main text, we also describe how some of them were validated by fitting the model to available experimental data (Fig. 2.3 in the main text).

The model parameters (Eqs. 2.3-2.4 in the main text) are listed in the table below:

Name	Unit	Description
e_M	h^{-1}	Constant characterizing nutrient composition of medium
k_R	h^{-1}	Rate constant of macromolecular synthesis
K_R	$\mathrm{g\ L}^{-1}$	Half-saturation constant of macromolecular synthesis
β	$\mathrm{L\ g}^{-1}$	Inverse of the cellular density of macromolecules
α	–	Resource allocation parameter

The values derived below are summarized in S1 Table.

e_M

By definition, e_M is the effective turnover of the metabolic macroreaction producing precursors from external substrates, obtained by dividing the reaction rate v_M by the enzyme concentration m (Eq. 2.6). The unit of e_M is min^{-1}, and can be decomposed as follows:

$$[e_M] = \frac{[\text{mass of metabolic product}]}{[\text{mass of enzyme M}] \cdot [\text{time}]} = \frac{1}{[\text{time}]}.$$

Note that $e_M = k_M\, s/(K_M + s)$ where k_M is a rate constant, indicating the maximal rate of conversion of external nutrients to precursor metabolites. e_M will thus vary with the concentration s of the external nutrients and the kind of nutrient. For example, the precursor mass that can be produced from 1 g of glucose is higher than that produced from 1 g of acetate.

How can we find a typical value for k_M, and thus for e_M (both have the same order of magnitude if we suppose that the reaction is not operating far below saturation, that is, $e_M \approx k_M$)? A reasonable estimate for k_M can be obtained from the turnover numbers of reactions involved in the synthesis of charged tRNA, since the latter are directly consumed by the most abundant part of the gene expression machinery, the ribosomes.

Ref. [80] provides a typical value for such a reaction, catalyzed by glutaminyl-tRNA synthetase: $k_{cat,GlnRS} = 3.2\ \mathrm{s}^{-1}$, indicating that on average 3.2 glutaminyl-tRNA molecules are produced per glutaminyl-tRNA synthetase molecule per second. After conversion to mass units using molar weight from [81], this yields

$$k_{cat,GlnRS} = \frac{3.2 \cdot 147}{64.4 \cdot 10^3} \approx 10^{-3}\ \text{g of glutaminyl-tRNA} \cdot \text{g of enzyme}^{-1} \cdot \text{s}^{-1}.$$

We therefore take

$$k_M \approx 3.6\ \text{h}^{-1},$$

and thus obtain an upper bound for e_M in our simulations.

k_R

k_R is the mass rate constant describing the maximal rate of conversion of precursors to macromolecules [h^{-1}]. As for e_M, we can decompose this into

$$[k_R] = \frac{[\text{mass of macromolecules}]}{[\text{mass of gene expression machinery}] \cdot [\text{time}]} = \frac{1}{[\text{time}]}$$

To obtain an order of magnitude for the mass of macromolecules, we focus on proteins since they are the most abundant macromolecules in the cell [28]. The dimensional analysis of k_R thus becomes:

$$\begin{aligned}
[k_R] &= \frac{[\text{protein mass produced}]}{[\text{ribosomal mass}] \cdot [\text{hour}]} \\
&= \frac{[\text{moles of protein}] \cdot [\text{protein molar mass}]}{[\text{moles of ribosome}] \cdot [\text{ribosome molar mass}] \cdot [\text{hour}]} \\
&= \frac{[\text{moles of amino acids}] \cdot [\text{molar mass of amino acids}]}{[\text{moles of ribosome}] \cdot [\text{hour}] \cdot [\text{ribosome molar mass}]} \\
&\approx \frac{[\text{maximal protein elongation rate}] \cdot [\text{molar mass of amino-acids}]}{[\text{ribosome molar mass}]}.
\end{aligned}$$

The values in the last equality are available from the literature [28,36,82,83]. We obtain

$$k_R \approx \frac{10 \cdot 100}{10^6} \cdot 3600 \approx 3.6\ \text{h}^{-1}.$$

This value is comparable with the translational capacity k_T, in μg of protein per μg of ribosomal protein per hour, given by Scott *et al.* [12]:

$$k_T = \frac{4.5\ \mu\text{g of protein / } \mu\text{g of RNA / h}}{0.76\ \mu\text{g of ribosomal protein / } \mu\text{g of RNA}} = 5.9\ \text{h}^{-1}.$$

K_R

A value for the parameter K_R, representing the half-saturation constant of macromolecular synthesis, is more difficult to obtain from the literature. However, assuming that ribosomes operate close to saturation (80% over a range of growth rates [28]), we find that $K_R \approx 0.25\,p$, with p the total amino acid concentration. The total concentration of amino acids in the cell is around 150 mmol L^{-1} [84], which with a mean molecular weight of 118.9 g mol^{-1} for amino acids [82], yields a mass concentration of 17.8 g L^{-1}. These considerations led to the following order of magnitude for K_R:

$$K_R \approx 1 \text{ g L}^{-1}.$$

β

β is the inverse of the cellular density of macromolecules, which has been shown constant during balanced growth over a large range of growth rates [85], and there is some data suggesting that β varies little during growth transitions as well [86]. From [87, 88] we take the following typical value for β:

$$\beta \approx \frac{1}{300} \approx 0.003 \text{ L g}^{-1}.$$

E_M and K

From the values of the parameter in the dimensional model, one can deduce the parameters in the nondimensional model used in the simulations:

$$E_M = \frac{e_M}{k_R} = \frac{3.6}{3.6} = 1 \quad , \quad K = \beta\, K_R = 3 \cdot 10^{-3} \cdot 1 = 0.003.$$

2.14 S3 Text – Solution of optimal control problem

2.14.1 Statement of the problem

We consider the dimensionless system defined by Eqs 2.11-2.12 in the main text, which are here repeated for clarity:

$$\begin{aligned} \frac{d\hat{p}}{d\hat{t}} &= (1-\hat{r})\,E_M - (1+\hat{p})\,\hat{r}\,\frac{\hat{p}}{K+\hat{p}}, \\ \frac{d\hat{r}}{d\hat{t}} &= \hat{r}\frac{\hat{p}}{K+\hat{p}}\,(\alpha(\hat{t})-\hat{r}). \end{aligned} \tag{2.61}$$

As stated in the section *Biomass maximization as an optimal control problem* in the main text, the objective of this study is to maximize the growth rate on an interval $[0,\tau]$ after a nutrient upshift. With Eq. **??** in S1 Text, we have

$$\hat{\mu} = \hat{r}\,\frac{\hat{p}}{K+\hat{p}}.$$

In order to avoid boundary effects occurring over finite time intervals, notably the depletion of precursors just before τ, we solve the optimal control problem over an infinite horizon ($\tau \to \infty$). Consider the set of admissible controls

$$\mathcal{U} = \{\alpha : \mathbb{R} \to [0,1] \;\mid\; \alpha(\cdot) \text{ measurable}\}.$$

The optimization problem can then be stated as follows:

$$\alpha_{opt} = \arg\max_{\alpha\in\mathcal{U}} J(\alpha) \equiv \int_0^{+\infty} \hat{r}(\hat{t})\frac{\hat{p}(\hat{t})}{K+\hat{p}(\hat{t})}d\hat{t}, \tag{2.62}$$

where $(\hat{p}(\hat{t}),\hat{r}(\hat{t}))$ is the unique solution of Eq. 2.61 starting at a given point $(\hat{p}_0,\hat{r}_0) \in \Omega \equiv \mathbb{R}_*^+ \times (0,1)$ for a given control $\alpha \in \mathcal{U}$.

Given that the performance index $J(\alpha)$ diverges, we actually consider *overtaking optimality* [40]. Consider the performance index of the trajectory $x(\cdot)$ emanating from x_0 and generated by $u(\cdot)$ defined for any $T \geq 0$ by

$$J_T(x_0,u(\cdot)) = \int_0^T f_0(x(t),u(t),t)dt.$$

A trajectory $x^*(\cdot)$ emanating from x_0 and generated by $u^*(\cdot)$ is said to be overtaking optimal if for any other trajectory $x(\cdot)$ emanating from x_0 and generated by $u(\cdot)$ the following holds

$$\liminf_{T\to\infty} \{J_T(x_0,u^*(\cdot)) - J_T(x_0,u(\cdot))\} \geq 0.$$

Roughly speaking, a trajectory is overtaking optimal if "the performance index catches up with the performance index of any other trajectory" [40].

2.14.2 Maximum Principle

Necessary conditions on optimal trajectories can be obtained by the Infinite Horizon Maximum Principle [40]. Let $H(\hat{p}, \hat{r}, \lambda_p, \lambda_r, \lambda_0, \alpha)$ be the Hamiltonian of the system, defined by

$$H(\cdot) \equiv \lambda_p \, E_M \, (1 - \hat{r}) - \hat{r} \, \frac{\hat{p}}{K + \hat{p}} \, [\lambda_p (1 + \hat{p}) + \lambda_r \, \hat{r} + \lambda_0] + \alpha \, \lambda_r \, \hat{r} \, \frac{\hat{p}}{K + \hat{p}}.$$

Moreover, let α be an optimal control, and $\hat{x}(\cdot) = (\hat{p}(\cdot), \hat{r}(\cdot))$ the associated trajectory. Then, there exists $\lambda_0 \leq 0$ and an absolutely continuous map $\lambda = (\lambda_p, \lambda_r) : [0, +\infty) \to \mathbb{R}^2$ such that $(\lambda, \lambda_0) \neq 0$, and

$$\dot{\lambda}_p = -\frac{\partial H}{\partial \hat{p}} = \hat{r} \, \frac{K}{(K + \hat{p})^2} \, [\lambda_p \, (1 + \hat{p}) + \lambda_r \, (\hat{r} - \alpha) + \lambda_0] + \hat{r} \, \frac{\hat{p}}{K + \hat{p}} \, \lambda_p, \tag{2.63}$$

$$\dot{\lambda}_r = -\frac{\partial H}{\partial \hat{r}} = \lambda_p \, E_M + \frac{\hat{p}}{K + \hat{p}} \, [\lambda_p \, (1 + \hat{p}) + \lambda_r \, (2\hat{r} - \alpha) + \lambda_0] \, . \tag{2.64}$$

The maximization condition is given by:

$$\begin{array}{l} \alpha(\hat{t}) \in \arg \ max_{v \in [0,1]} H(\hat{x}(\hat{t}), \lambda(\hat{t}), \lambda_0, v), \\ \text{almost everywhere on } [0, +\infty). \end{array} \tag{2.65}$$

An extremal trajectory is a quadruplet $(\hat{x}(\cdot), \lambda(\cdot), \lambda_0, \alpha(\cdot))$ satisfying Eqs 2.61-2.65. The extremal is said to be normal (resp. abnormal) if $\lambda_0 < 0$ (resp. $\lambda_0 = 0$). In the normal case, we normalize the adjoint vector so that $\lambda_0 = -1$.

From Eq. 2.65, it follows that the control strategy is given by the sign of the *switching function* $\phi(\cdot) \equiv \lambda_r \, \hat{r} \, \hat{p}/(K + \hat{p})$, that is,

$$\begin{cases} \alpha = 1 \iff \phi(\cdot) > 0, \\ \alpha = 0 \iff \phi(\cdot) < 0. \end{cases}$$

Finally, given that the system is autonomous, the Hamiltonian is conserved along any extremal trajectory.

2.14.3 Characterization of singular arcs

Whenever ϕ is vanishing over a time interval, we say that the trajectory is *singular*. We will now characterize such trajectories. If $I = [\hat{t}_1, \hat{t}_2]$ is a singular arc, we have $\phi(\hat{t}) = \dot{\phi}(\hat{t}) = 0$, for all $\hat{t} \in [\hat{t}_1, \hat{t}_2]$, that is, $\lambda_r(\hat{t}) = 0$ and $\dot{\lambda}_r(\hat{t}) = 0$.

For abnormal extremal trajectories, we get $\lambda_p(\hat{t}) = 0$, in contradiction with the Maximum Principle, so there is no singular arc. An abnormal extremal trajectory is therefore a concatenation of bang arcs.

For normal extremal trajectories, using additionally that H is constant along an extremal trajectory, we obtain that λ_p is constant along a singular arc. By combining $\dot{\lambda}_p = 0$ and $\dot{\lambda}_r = 0$, we obtain $\hat{p}(\hat{t}) = \sqrt{E_M\, K} = \hat{p}^*_{opt}$. Using $d\hat{p}/d\hat{t} = 0$, we finally get $\hat{r}(\hat{t}) = \hat{r}^*_{opt}$. Thus, the singular arc is the optimal steady state, corresponding to a singular control $\alpha(\hat{t}) = \alpha^*_{opt}$, with α^*_{opt} depending on E_M (S1 Text).

A necessary condition of optimality for a singular arc is given by the Kelley condition [76]. We must differentiate ϕ with respect to $\hat{t}$ until α appears in the derivative. Along a singular arc, we obtain for $q = 2$:

$$(-1)^q \frac{\partial}{\partial \alpha} \frac{d^{2q}}{d\hat{t}^{2q}} \phi(\hat{t}) < 0,$$

satisfying the Kelley condition necessary for optimality. Given that the singular arc is of second order, an optimal trajectory can enter into the singular arc only by a *chattering arc* (also called the Fuller's phenomenon, *i.e.*, an arc with an infinite number of switches [76, 89]).

2.14.4 Analysis of the adjoint system

Recalling that a switch corresponds to a change of sign of λ_r, the analysis of the adjoint system (Eqs 2.63-2.64) may be useful to characterize the switches of extremal trajectories.

First, for the abnormal case, we can easily determine in the phase-plane the possible transitions between the four regions defined by the axes (see Fig. 2.10). A trajectory can cross at most twice the λ_p-axis, so we conclude that an abnormal extremal cannot have more than two switches. Thus, an abnormal extremal is a concatenation of at most three bang arcs ($\alpha(t) = 0$ or $\alpha(t) = 1$). When $\alpha(t) = 0$ or $\alpha(t) = 1$ for a long time, the growth rate tends to zero. We therefore conclude that abnormal extremal trajectories are not optimal.

Secondly, for the normal case, after the first switch, a trajectory with two consecutive switches in the regions $\{(\hat{p},\hat{r}) \in \Omega \mid \hat{p} < \hat{p}^*_{opt}\}$ or $\{(\hat{p},\hat{r}) \in \Omega \mid \hat{p} > \hat{p}^*_{opt}\}$ is not possible, as shown in Fig. 2.10. Therefore, such a trajectory is not optimal given that it does not fulfill the conditions given by the Maximum Principle. We conclude that if the optimal trajectory has a concatenation of bang arcs, the switches must alternatingly occur in the regions $\{(\hat{p},\hat{r}) \in \Omega \mid \hat{p} < \hat{p}^*_{opt}\}$ and $\{(\hat{p},\hat{r}) \in \Omega \mid \hat{p} > \hat{p}^*_{opt}\}$.

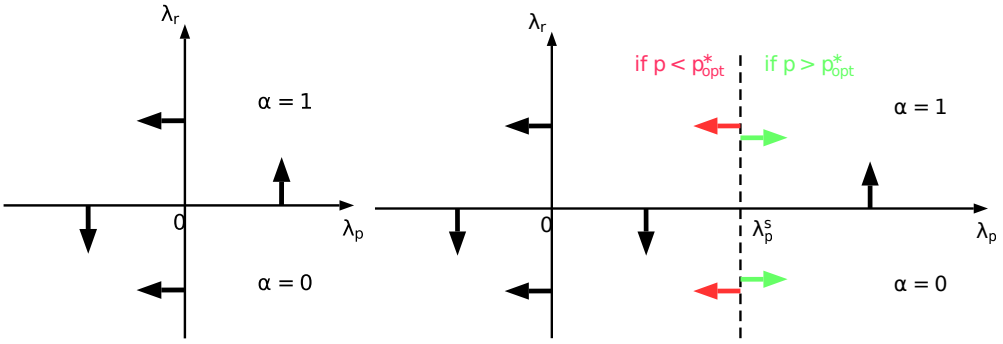

Figure 2.10 – **Transitions between regions in the phase-plane for the adjoint system.** A switch occurs when a trajectory crosses the λ_p-axis. Left: abnormal case. An extremal trajectory cannot have more than two switches. Right: normal case. $(\lambda^s_p, 0)$ corresponds to the singular arc. After the first switch, an extremal trajectory cannot have two consecutive switches if it stays in the region $\{(\hat{p},\hat{r}) \in \Omega \mid \hat{p} < \hat{p}^*_{opt}\}$ or $\{(\hat{p},\hat{r}) \in \Omega \mid \hat{p} > \hat{p}^*_{opt}\}$.

2.14.5 Optimal trajectories

From the Maximum Principle, we have shown that the optimal trajectory is a concatenation of bang arcs ($\alpha(t) = 0$ or $\alpha(t) = 1$) and possibly a singular arc corresponding to the optimal steady state $(\hat{p}(\hat{t}), \hat{r}(\hat{t})) = (\hat{p}^*_{opt}, \hat{r}^*_{opt})$. Moreover, if the optimal trajectory has a singular arc, it must enter it through a chattering arc (*i.e.*, with an infinite number of switches between $\alpha = 0$ and $\alpha = 1$).

These elements motivate the supposition that optimal solutions consist in a transient (chattering arc) towards the optimal steady state, after which they remain there (until the next change of environment). The chattering arc can be characterized by a switching curve $\hat{p} \mapsto \varphi(\hat{p})$ which passes through the optimal steady state. Defining A_0 and A_1 the regions above and below φ in the $(\hat{p},\hat{r})$-plane, respectively, we conjecture that the following feedback control law is optimal:

$$\begin{cases} \alpha(\hat{t}) = 0 \text{ if } (\hat{p}(\hat{t}), \hat{r}(\hat{t})) \in A_0, \\ \alpha(\hat{t}) = 1 \text{ if } (\hat{p}(\hat{t}), \hat{r}(\hat{t})) \in A_1, \\ \alpha(\hat{t}) = \alpha_{opt} \text{ if } (\hat{p}(\hat{t}), \hat{r}(\hat{t})) = (\hat{p}^*_{opt}, \hat{r}^*_{opt}). \end{cases} \tag{2.66}$$

Loosely speaking, the chattering arc corresponds to a spiral composed of bang arcs wrapping around the optimal steady state, where the switches alternatingly occur in the regions $\{(\hat{p}, \hat{r}) \in \Omega \mid \hat{p} < \hat{p}^*_{opt}\}$ and $\{(\hat{p}, \hat{r}) \in \Omega \mid \hat{p} > \hat{p}^*_{opt}\}$, in line with the analysis of the adjoint system. This is a first hint that the proposed control strategy is optimal. Moreover, our conjecture is also in line with the *turnpike property*: Trélat and Zuazua [90] have shown that, for quite a generic class of systems, the optimal strategy consists in staying at the optimal steady state (after a short transient).

As explained in the *Methods* section of the main text, we numerically solved the optimal control problem by the direct method using the `bocop` software [41]. It is important to stress that the optimization process was performed without any preliminary assumptions on the characteristics of the optimal trajectory. The fact that the numerical solution verifies the Maximum Principle (*i.e.*, the singular arc corresponds to the optimal steady state) and the Kelley condition (*i.e.*, the presence of a chattering arc) tends to confirm that the control strategy of Eq. 2.66 is optimal. As an aside, we note that due to the fact that numerical optimization was performed for a finite horizon, we actually obtained a second chattering arc escaping from the singular arc at the end of the simulation. This is a classical property of the turnpike strategy: the optimal trajectory leaves the optimal steady state just before the end of the time interval of interest, in our case consuming almost all precursors. This arc was removed from the plot in Fig. 2.4, because it does not occur with an infinite horizon and is therefore a numerical artifact for this study.

2.15 S4 Text – Kinetic model of the ppGpp system in *Escherichia coli*

The recently published model of Bosdriesz *et al.* [17] provides a synthesis of the currently available knowledge of the ppGpp regulatory system. Through the mechanisms of ppGpp production and degradation, it describes regulation of the synthesis of ribosomal RNA. We explain below how we use the model to compare the action of the ppGpp system with the on-off control strategy. The denomination of variables and parameters follows the Supporting Information of [17] , and is reproduced in Table **??** in order to make the text self-contained.

The evolution of the cellular concentration of ppGpp is described in [17] by

$$\frac{d\texttt{ppGpp}}{dt} = v_{RelA}(r_{t,tot}) + v_{spoT} - k_{spoT} \cdot \texttt{ppGpp}, \tag{2.67}$$

where v_{spoT} and k_{spoT} are constants (see Table **??**), and v_{RelA} is a function of $r_{t,tot}$, the total concentration of "stalled" ribosomes:

$$v_{RelA}(r_{t,tot}) = k_{RelA} \cdot RelA_{tot} \cdot \frac{r_{t,tot}}{K_{D,RelA} + r_{t,tot}}. \tag{2.68}$$

The amount of stalled ribosomes is determined by the equilibrium between charged and uncharged tRNA, t_{ai} and t_i, in the cell:

$$r_{t,tot} = \sum_i r_{ti} = \sum_i r_i \frac{t_i/\kappa_t}{1 + t_{ai}/\kappa_{ta} + t_i/\kappa_t}, \tag{2.69}$$

which can be rewritten as

$$r_{t,tot} = \sum_i r_i \frac{t_i/\kappa_t}{1 + (0.5r - t_i)/\kappa_{ta} + t_i/\kappa_t}, \tag{2.70}$$

using the assumption that $t_{tot,i} = t_{ai} + t_i = 0.5 \cdot r$. r_i denotes the concentration of ribosomes recognizing amino acid i. Finally, with $r = \sum_i r_i$ the total ribosome concentration and a_i the concentration of amino acid i, the dynamics of the charged tRNA concentration is described by

$$\frac{dt_{ai}}{dt} = v_{tai}(a_i, t_i) - f_i \cdot v_{ribosome}(t_i, r), \tag{2.71}$$

with $v_{tai}(a_i, t_i)$ the synthesis rate of charged tRNA, and $f_i \cdot v_{ribosome}(t_i, r)$

their consumption via protein synthesis. In particular,

$$v_{tai}(a_i, t_i) = k_{Si} \cdot S_{tot,i} \cdot \frac{t_i\, a_i}{t_i\, K_{Mai} + a_i\, K_{Mti} + t_i\, a_i}, \tag{2.72}$$

$$v_{ribosome}(t_i, r) = k_{rib} \cdot r \cdot \left(1 + \sum_i \left[f_i \cdot \left(1 + \frac{t_i}{\kappa_t}\right) \frac{\kappa_{ta}}{0.5 \cdot r - t_i}\right]\right)^{-1} \tag{2.73}$$

For comparison with our framework, we need `ppGpp` as a direct function of the total amino acid concentration $a = \sum_i a_i$ (a proxy for precursors) and total ribosome concentration r (a proxy for gene expression machinery). To this end, we made two additionnal assumptions:

(A1) All concentrations specific to one type of amino acid i (a_i, t_{ai}, t_i, r_i) are in the same proportion $f_i = f = 1/20$ with respect to the total concentrations (a, t_a, t, r).

(A2) We apply a quasi-steady-state approximation (QSSA) to the dynamics of the concentration of the charged tRNAs (t_{ai}) and the concentration of ppGpp (`ppGpp`). That is, the dynamics of these variables are assumed fast relative to the dynamics of the amino acid concentrations (a_i) and the total ribosome concentration (r).

Using (A2), we can rewrite Eq. 2.71 as follow:

$$v_{tai}(a_i, t_i) = f_i \cdot v_{ribosome}(t_i, r), \tag{2.74}$$

which, using (A1) and Eqs 2.72 and 2.73, leads to:

$$k_{Si} \cdot S_{tot,i} \cdot \frac{t_i\, a_i}{t_i\, K_{Mai} + a_i\, K_{Mti} + t_i\, a_i} = f_i \cdot k_{rib} \cdot r \cdot \left(1 + \frac{\kappa_{ta}}{0.5r - t_i} \cdot \left(1 + \frac{t_i}{\kappa_t}\right)\right)^{-1}. \tag{2.75}$$

By rearranging both sides of the equation, t_i can be expressed as a function of a_i and r, which yields:

$$\begin{aligned} &{t_i}^2 + B t_i + C = 0, \quad \text{with} \\ &A = \frac{k_{Si}\, S_{tot,i}\, a_i}{f_i\, k_{rib}\, r}\left(\frac{\kappa_{ta}}{\kappa_t} - 1\right) + K_{Mai} + a_i, \\ &B = \frac{k_{Si}\, S_{tot,i}\, a_i}{f_i\, k_{rib}\, r}(0.5\, r + \kappa_{ta}) + a_i\, K_{Mti} - 0.5\, r\, (K_{Mai} + a_i), \\ &C = -0.5\, r\, a_i\, K_{Mti}, \end{aligned} \tag{2.76}$$

and therefore

$$t_i(a_i, r) = \frac{-B \pm \sqrt{B^2 - 4AC}}{2A}.$$

It is not difficult to show that the only solution on $[0, 0.5\,r]$ is

$$t_i(a_i, r) = \frac{-B + \sqrt{B^2 - 4AC}}{2A}. \tag{2.77}$$

From this result, we obtain $r_{t,tot}$ as a function of a_i and r, by applying (A1) to Eq. **??**:

$$r_{t,tot}(t_i, r) = r \cdot \frac{t_i/\kappa_t}{1 + (0.5r - t_i)/\kappa_{ta} + t_i/\kappa_t}, \tag{2.78}$$

and substituting t_i by the expression of Eq. 2.77.

Finally, we apply (A2) to Eq. 2.67 and obtain the final expression giving the concentration of ppGpp as a function of the total amino acid and ribosome concentrations:

$$\texttt{ppGpp}(a_i, r) = \frac{1}{k_{spoT}} \left(k_{RelA} \cdot RelA_{tot} \cdot \frac{r_{t,tot}(a_i, r)}{K_{D,RelA} + r_{t,tot}(a_i, r)} + v_{spoT} \right). \tag{2.79}$$

This function is represented in Fig. **??** with parameters taken from Table 2.1.

The plotted surface of the function resembles the inverse of the on-off control strategy in Fig. 2.8, as expected, bearing in mind that ppGpp has an inhibitory effect on the synthesis of ribosomal RNA. We assumed a Michaelis-Menten inhibition for the regulatory effect of ppGpp on rRNA synthesis, and thus indirectly on the synthesis of ribosomal proteins [31, 47]:

$$\alpha(\texttt{ppGpp}) = \frac{K_I}{K_I + \texttt{ppGpp}}. \tag{2.80}$$

The inhibitory constant K_I lies in the dynamical range of variation of ppGpp. In Fig. 2.8 in the main text, we took $K_I = 10\ \mu$M.

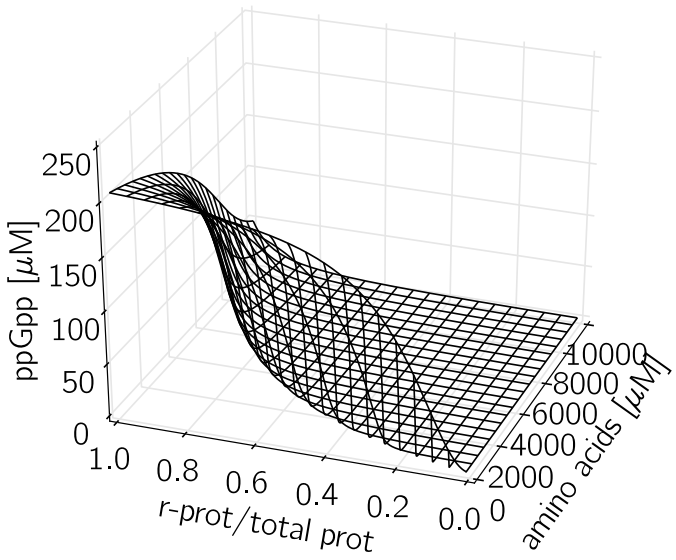

Figure 2.11 – **ppGpp concentration is a function of total ribosome and amino acid concentrations.**
We assume the dynamics of ppGpp to be fast on the time-scale of changes in the ribosome and amino acid concentrations. The concentration of ppGpp can thus be expressed as a function of the latter two variables, using the model of Bosdriesz *et al.* [17]. Parameters are taken from Table 2.1.

Symbol	Value	Unit	Description
a_i	–	μM	Concentration of aa i (not incorporated in protein)
t_{ai}	–	μM	Concentration of tRNA charged with aa i
t_i	–	μM	Concentration of free tRNA conjugate to aa i
$t_{tot,i}$	$0.5 \cdot r$	μM	Total concentration of tRNA conjugate to aa i
r_i	–	μM	Total concentration of ribosome with an A-site for aa i
r_{ti}	–	μM	Ribosomes with uncharged tRNA in an A-site for aa i
ppGpp	–	μM	Concentration of ppGpp
a	$\sum_i a_i$	μM	Total concentration of aa (not incorporated in protein)
t_a	$\sum_i t_{ai}$	μM	Total concentration of tRNA charged with aa
t	$\sum_i t_i$	μM	Total concentration of free tRNA
$r_{t,tot}$	$\sum_i r_{ti}$	μM	Total concentration of uncharged tRNA bound to ribosomes
r	$\sum_i r_i$	μM	Total concentration of ribosomes
v_{RelA}	–	μM/s	Rate of RelA-catalyzed ppGpp synthesis
v_{SpoT}	10^{-3}	μM/s	Rate of ppGpp synthesis by SpoT
v_{tai}	–	μM/s	Rate of amino-acyl tRNA i synthetase
$v_{ribosome}$	–	μM/s	Total rate of protein synthesis
k_{rib}	20	s^{-1}	k_{cat} of protein elongation
k_{RelA}	75	s^{-1}	k_{cat} of ppGpp synthesis by RelA
$K_{D,RelA}$	0.26	μM	Michaelis constant of RelA-catalyzed ppGpp production
$RelA_{tot}$	1/15	μM	RelA concentration
k_{SpoT}	$\ln(2)/30$	s^{-1}	Rate of ppGpp degradation by SpoT
κ_t	500	μM	Dissociation constant of uncharged tRNA-ribosome complex
κ_{ta}	1	μM	Dissociation constant of charged tRNA-ribosome complex
k_{Si}	100	s^{-1}	k_{cat} of aminoacyl-tRNA synthetase
$S_{tot,i}$	1	μM	Total concentration of aminoacyl-tRNA synthetase for aa i
K_{Mai}	100	μM	Michaelis constant of aa-tRNA synthetase for amino acids
K_{Mti}	1	μM	Michaelis constant of aa-tRNA synthetase for uncharged tRNA
f_i	1/20	–	Proportion of aa i in proteins (Assumption A1)

Table 2.1 – **Parameters and variables reused from Bosdriesz *et al.* [17]**. The abbreviation aa denotes amino acids.

2.16 S1 Table – Parameter values of self-replicator model

Parameter	Unit	Literature value	Fitted value
γ	–	No value	1.39
k_R	h^{-1}	3.6	2.23
e_M for M63+glycerol	h^{-1}	< 3.6	0.587
e_M for M63+glucose	h^{-1}	< 3.6	0.867
e_M for cAA+glycerol	h^{-1}	< 3.6	1.07
e_M for cAA+glucose	h^{-1}	< 3.6	1.57
e_M for RDM+glycerol	h^{-1}	< 3.6	3.48
e_M for RDM+glucose	h^{-1}	< 3.6	4.76
βK_R	–	0.003	Not fitted

Table 2.2 – **Parameter values of self-replicator model** The parameter values in the model were obtained by fitting Eq. 2.25 to the data of Scott et al [12] (Fig. 2.3 in the main text), as described in the *Methods* section. They are compared with order-of-magnitude estimates from the literature (S2 Text).

2.17 S1 Figure – Simple control strategies for the self-replicator of bacterial growth

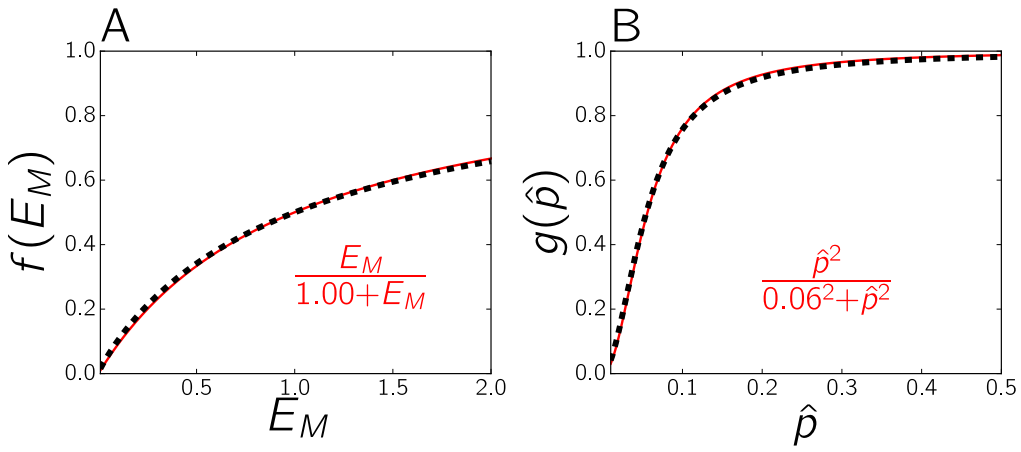

Figure 2.12 – *A:* Nutrient-only strategy: $\alpha = f(E_M)$. The dashed, black curve is the (unique) strategy driving the system exactly to the optimal steady state, that is, the state in which growth occurs at the maximal rate supported by E_M. The function f is defined by Eq. 2.27 in the *Methods* section of the main text. The solid, red curve is an approximation of this function by the simple Michaelis-Menten curve of Eq. 2.16, with $K_{mE} = 1.0$. *B:* Precursor-only strategy: $\alpha = g(\hat{p})$. The dashed, black curve is the (unique) strategy driving the system exactly to the optimal steady state. The function g is defined by Eq. 2.28 in the *Methods* section of the main text. The solid, red curve is an approximation of this function by the simple Hill curve of Eq. 2.18, with $K_{mp} = 0.06$ and a cooperativity coefficient 2.

Chapter 3

Monitoring of Gene Expression Machinery during growth transitions

Missing results as of today:
— manual segmentation of one well –> mean RFU per pixel per cell (2-3 days in the best case, it could be difficult to export schnitzcells data)
— semi-manual tracking of cells based on segmentation (hard to evaluate, will depend on schnitzcells performances, not optimistic)
— estimation of α and μ over time (2-3 days for calculation, 2-3 days for implementation). I need tracking for μ, maybe not for α
— make another experiments glu-sugar-glu (glycerol?), depends on Irina
— analyze this experiments (repeat steps above, will probably be faster if we manage to work everything out, but still takes time because it's manual)
— model modification to take into account the new data (5 days)
What could go wrong: everything. In particular:
— segmentation results could be impossible to export
— tracking might not work (schnitzcells not designed to handle massive cell disappearance)
— μ might be too noisy due to pixel size (note: image interpolation before segmentation might be a solution)
— what we saw on the rough analysis might just be an artefact (as Hans usually says "When it works the first time, something went horribly wrong.")
— the second experiment might not work (poor preculture, device plugged, out of focus overnight, medium contamination...)
Would everything go right, the chapter/article would be as follow.

3.1 Introduction

— Understanding growth transitions is important, because so and so.
— We predicted earlier counter-intuitive bang-bang-singular behaviours for GEM during transition
— But we're missing experimental data on what really happens in real cells during these transitions (quick review of available data)
— We fix it by making a strain with fluorescent ribosomes and monitoring ribosome abundance during growth transitions in a microfluidic device.

3.2 Methods

3.2.1 Strain design

We used rpsB, GFP, and a chromosomic construction because so and so.

3.2.2 Strain construction

We used Gibson assembly, Kan-pbad-ccdb, etc and obtain the following sequence.

3.2.3 Microfluidic device

Mother machine because needed to change the medium, single cell data because asynchronization etc.

3.2.4 Data analysis

We used this and that to analyze the microscopic images. We applied the following corrections.

3.3 Results

3.3.1 Model calibration

We want to get $\alpha(t)$ during a transition. We show that α can be obtained if we measure so and so.

3.3.2 Bang-bang expression during transitions, as predicted

One stunning figure that show the RFU / cell / pixels, and the predicted α for the glucose-acetate transition.

3.3.3 Discrepancies with the model and model adaptation

The growth rate stalls after the addition of glucose, which was not originally predicted by the model. This is because so and so. This can be taken into account if we add another sector (M1 and M2). This raises a new interesting question : during the transition amino-acids drop, so the cell should produce ribosomes, but it also need to produce the new enzymes to actually be able to perform metabolism. We thus have competition between several layers of regulation, which can be added to the model by doing so and so.

3.4 Discussion

More research need to be done.

Could be interesting to use transitions for syn bio purposes. Could be interesting to validate such results in different microorganisms, with different type of medium (fast env, slow env, etc)

3.5 Supporting Information

— Strain validation (signal-to-noise ratio, growth rate not hampered in microplate reader)
— Primers used for gibson assembly
— Difference between mCherry and GFP (mCherry not good because so and so, GFP was chosen)

Chapter 4

Discussion

- in praise of simple models - an intrinsic link between complexity and environment dynamic - some perspectives for industrial production

Bibliography

1. Schaechter M, Ingraham JL, Neidhardt FC. Microbe. ASM Press; 2006. doi: 10.1128/9781555813208.
2. Keseler IM, Mackie A, Peralta-Gil M, Santos-Zavaleta A, Gama-Castro S, Bonavides-Martínez C, et al. EcoCyc: fusing model organism databases with systems biology. Nucleic Acids Res. 2013 Jan;41(Database issue):D605–12. doi: 10.1093/nar/gks1027.
3. Frank SA. The trade-off between rate and yield in the design of microbial metabolism. J Evol Biol. 2010 Mar;23(3):609–13. doi: 10.1111/j.1420-9101.2010.01930.x.
4. MacLean RC. The tragedy of the commons in microbial populations: insights from theoretical, comparative and experimental studies. Heredity. 2008 May;100(5):471–7. doi: 10.1038/sj.hdy.6801073.
5. Schuetz R, Zamboni N, Zampieri M, Heinemann M, Sauer U. Multidimensional optimality of microbial metabolism. Science. 2012 May;336(6081):601–4. doi: 10.1126/science.1216882.
6. Schuster S, Pfeiffer T, Fell D. Is maximization of molar yield in metabolic networks favoured by evolution? J Theor Biol. 2008 Jun;252(3):497–504. doi: 10.1016/j.jtbi.2007.12.008.
7. Schuetz R, Kuepfer L, Sauer U. Systematic evaluation of objective functions for predicting intracellular fluxes in *Escherichia coli*. Mol Syst Biol. 2007 Jan;3:119. doi: 10.1038/msb4100162.
8. Edwards JS, Ibarra RU, Palsson BO. In silico predictions of *Escherichia coli* metabolic capabilities are consistent with experimental data. Nat Biotechnol. 2001 Feb;19(2):125–30. doi: 10.1038/84379.
9. Ibarra RU, Edwards JS, Palsson BO. *Escherichia coli* K-12 undergoes adaptive evolution to achieve in silico predicted optimal growth. Nature. 2002 Nov;420(6912):186–9. doi: 10.1038/nature01149.
10. Lewis NE, Hixson KK, Conrad TM, Lerman JA, Charusanti P, Polpitiya AD, et al. Omic data from evolved *E. coli* are consistent with

computed optimal growth from genome-scale models. Mol Syst Biol. 2010 Jul;6:390. doi: 10.1038/msb.2010.47.

11. Molenaar D, van Berlo R, de Ridder D, Teusink B. Shifts in growth strategies reflect tradeoffs in cellular economics. Mol Syst Biol. 2009 Jan;5:323. doi: 10.1038/msb.2009.82.

12. Scott M, Gunderson CW, Mateescu EM, Zhang Z, Hwa T. Interdependence of cell growth and gene expression: origins and consequences. Science. 2010 Nov;330(6007):1099–102. doi: 10.1126/science.1192588.

13. Scott M, Klumpp S, Mateescu EM, Hwa T. Emergence of robust growth laws from optimal regulation of ribosome synthesis. Mol Syst Biol. 2014 Aug;10:747. doi: 10.15252/msb.20145379.

14. Servedio MR, Brandvain Y, Dhole S, Fitzpatrick CL, Goldberg EE, Stern CA, et al. Not just a theory—the utility of mathematical models in evolutionary biology. PLoS Biol. 2014 Dec;12(12):e1002017. doi: 10.1371/journal.pbio.1002017.

15. Maitra A, Dill KA. Bacterial growth laws reflect the evolutionary importance of energy efficiency. Proc Natl Acad Sci USA. 2014 Dec;112(2):406–11. doi: 10.1073/pnas.1421138111.

16. Kremling A, Geiselmann J, Ropers D, de Jong H. Understanding carbon catabolite repression in *Escherichia coli* using quantitative models. Trends Microbiol. 2015;23(2):99–109. doi: 10.1016/j.tim.2014.11.002.

17. Bosdriesz E, Molenaar D, Teusink B, Bruggeman FJ. How fast-growing bacteria robustly tune their ribosome concentration to approximate growth-rate maximization. FEBS J. 2015 Mar;282:2029–204. doi: 10.1111/febs.13258.

18. Weiße AY, Oyarzún DA, Danos V, Swain PS. Mechanistic links between cellular trade-offs, gene expression, and growth. Proc Natl Acad Sci USA. 2015 Mar;112(9):1038–47. doi: 10.1073/pnas.1416533112.

19. Fishov I, Zaritsky A, Grover NB. On microbial states of growth. Mol Microbiol. 1995 Mar;15(5):789–94. doi: 10.1111/j.1365-2958.1995.tb02349.x.

20. Borirak O, Bekker M, Hellingwerf KJ. Molecular physiology of the dynamic regulation of carbon catabolite repression in *Escherichia coli*. Microbiology. 2014 Jun;160(Pt6):1214–23. doi: 10.1099/mic.0.077289-0.

21. Savageau MA. *Escherichia coli* habitats, cell types, and molecular mechanisms of gene control. Am Nat. 1983 Dec;122(6):732–44.

22. Savageau MA. Demand theory of gene regulation. II. Quantitative application to the lactose and maltose operons of *Escherichia coli*. Genetics. 1998 Jan;149(4):1677–91.
23. Blount ZD. The unexhausted potential of *E. coli*. eLife. 2015 Mar;4:e05826. doi: 10.7554/eLife.05826.
24. van Elsas JD, Semenov AV, Costa R, Trevors JT. Survival of *Escherichia coli* in the environment: fundamental and public health aspects. ISME J. 2011 Feb;5(2):173–83. doi: 10.1038/ismej.2010.80.
25. Pavlov MY, Ehrenberg M. Optimal control of gene expression for fast proteome adaptation to environmental change. Proc Natl Acad Sci USA. 2013 Dec;110(51):20527–32. doi: 10.1073/pnas.1309356110.
26. van den Berg HA, Kiselev YN, Kooijman SaLM, Orlov MV. Optimal allocation between nutrient uptake and growth in a microbial trichome. J Math Biol. 1998 Jul;37(1):28–48. doi: 10.1007/s002850050118.
27. Waldherr S, Oyarzún DA, Bockmayr A. Dynamic optimization of metabolic networks coupled with gene expression. J Theor Biol. 2015 Jan;365:469–85. doi: 10.1016/j.jtbi.2014.10.035.
28. Ehrenberg M, Bremer H, Dennis PP. Medium-dependent control of the bacterial growth rate. Biochimie. 2013 Apr;95(4):643–58. doi: 10.1016/j.biochi.2012.11.012.
29. Stengel RF. Optimal Control and Estimation. Mineola, NY: Dover Publications; 1994.
30. Dalebroux ZD, Swanson MS. ppGpp: magic beyond RNA polymerase. Nat Rev Microbiol. 2012;10(3):203–12. doi: 10.1038/nrmicro2720.
31. Potrykus K, Cashel M. (p)ppGpp: still magical? Annu Rev Microbiol. 2008;62:35–51. doi: 10.1146/annurev.micro.62.081307.162903.
32. Hauryliuk V, Atkinson GC, Murakami KS, Tenson T, Gerdes K. Recent functional insights into the role of (p)ppGpp in bacterial physiology. Nat Rev Microbiol. 2015;13(5):298–309. doi: 10.1038/nrmicro3448.
33. Iglesias PA, Ingalls BP. Control Theory and Systems Biology. MIT Press; 2010.
34. Sipper M. Fifty years of research on self-replication: an overview. Artif Life. 1998;4(3):237–57. doi: 10.1162/106454698568576.
35. Flamm C, Endler L, Müller S, Widder S, Schuster P. A minimal and self-consistent in silico cell model based on macromolecular interactions. Philos Trans R Soc B. 2007;362(1486):1831–9. doi: 10.1098/rstb.2007.2075.

36. Klumpp S, Scott M, Pedersen S, Hwa T. Molecular crowding limits translation and cell growth. Proc Natl Acad Sci USA. 2013 Oct;110(42):16754–9. doi: 10.1073/pnas.1310377110.

37. Kjeldgaard NO. The kinetics of ribonucleic acid- and protein formation in *Salmonella typhimurium* during the transition between different states of balanced growth. Biochim Biophys Acta. 1961 Apr;49(1):64–76. doi: 10.1016/0006-3002(61)90870-8.

38. Schaechter M. Patterns of cellular control during unbalanced growth. Cold Spring Harb Symp Quant Biol. 1961 Jan;26:53–62. doi: 10.1101/SQB.1961.026.01.011.

39. Johnsen K, Molin S, Karlström O, Maaløe O. Control of protein synthesis in *Escherichia coli*: analysis of an energy source shift-down. J Bacteriol. 1977 Jan;131(1):18–29.

40. Carlson DA, Haurie AB, Leizarowitz A. Infinite Horizon Optimal Control. Berlin, Heidelberg: Springer; 1991. doi: 10.1007/978-3-642-76755-5.

41. Bonnans F, Martinon P, Grélard V. Bocop - A collection of examples; 2012. Eprint: https://hal.inria.fr/hal-00726992.

42. Chubukov V, Gerosa L, Kochanowski K, Sauer U. Coordination of microbial metabolism. Nat Rev Microbiol. 2014 Mar;12:327–40. doi: 10.1038/nrmicro3238.

43. Deutscher J, Francke C, Postma PW. How phosphotransferase system-related protein phosphorylation regulates carbohydrate metabolism in bacteria. Microbiol Mol Biol Rev. 2006;70(4):939–1031. doi: 10.1128/MMBR.00024-06.

44. Görke B, Stülke J. Carbon catabolite repression in bacteria: many ways to make the most out of nutrients. Nat Rev Microbiol. 2008;6(8):613–24. doi: 10.1038/nrmicro1932.

45. English BP, Hauryliuk V, Sanamrad A, Tankov S, Dekker NH, Elf J. Single-molecule investigations of the stringent response machinery in living bacterial cells. Proc Natl Acad Sci USA. 2011;108(31):365–73. doi: 10.1073/pnas.1102255108.

46. Dennis PP, Ehrenberg M, Bremer H. Control of rRNA synthesis in *Escherichia coli*: a systems biology approach. Microbiol Mol Biol Rev. 2004 Jan;68(4):639–68. doi: 10.1128/MMBR.68.4.639-668.2004.

47. Keener J, Nomura M. Regulation of ribosome synthesis. In: Neidhardt FC, III RC, Ingraham JL, Lin ECC, Low KB, Magasanik B, et al., editors. *Escherichia coli* and *Salmonella*: Cellular and Molecular Biology. 2nd ed. Washington, DC: ASM Press; 1996. p. 1417–31.

48. Bremer H, Dennis P. Modulation of chemical composition and other parameters of the cell by growth rate. In: Neidhardt FC, III RC, Ingraham JL, Lin ECC, Low KB, Magasanik B, et al., editors. *Escherichia coli* and *Salmonella*: Cellular and Molecular Biology. 2nd ed. Washington, DC: ASM Press; 1996. p. 1553–69.

49. Murray HD, Schneider DA, Gourse RL. Control of rRNA expression by small molecules is dynamic and nonredundant. Mol Cell. 2003;12(1):125–34. doi: 10.1016/S1097-2765(03)00266-1.

50. Scott M, Hwa T. Bacterial growth laws and their applications. Curr Opin Biotechnol. 2011 Aug;22(4):559–65. doi: 10.1016/j.copbio.2011.04.014.

51. Macevicz S, Oster G. Modeling social insect populations II: Optimal reproductive strategies in annual eusocial insect colonies. Behav Ecol Sociobiol. 1976;1(3):265–82. doi: 10.1007/BF00300068.

52. Itzkovitz S, Blat IC, Jacks T, Clevers H, van Oudenaarden A. Optimality in the development of intestinal crypts. Cell. 2012 Feb;148(3):608–19. doi: 10.1016/j.cell.2011.12.025.

53. Bartl M, Li P, Schuster S. Modelling the optimal timing in metabolic pathway activation—Use of Pontryagin's Maximum Principle and role of the Golden section. Biosystems. 2010 Jul;101(1):67–77. doi: 10.1016/j.biosystems.2010.04.007.

54. Oyarzún DA, Ingalls BP, Middleton RH, Kalamatianos D. Sequential activation of metabolic pathways: a dynamic optimization approach. Bull Math Biol. 2009;71:1851–72. doi: 10.1007/s11538-009-9427-5.

55. Madar D, Dekel E, Bren A, Zimmer A, Porat Z, Alon U. Promoter activity dynamics in the lag phase of *Escherichia coli*. BMC Syst Biol. 2013 Dec;7(1):136. doi: 10.1186/1752-0509-7-136.

56. Kiselev YN, Avvakumov SN, Orlov MV. Resource allocation problem in a two-sector economic model of special form. Differ Equ. 2009 Dec;45(12):1791–810. 00003. doi: 10.1134/S0012266109120106.

57. Potrykus K, Murphy H, Philippe N, Cashel M. ppGpp is the major source of growth rate control in *E. coli*. Environ Microbiol. 2011;13(3):563–75. doi: 10.1111/j.1462-2920.2010.02357.x.

58. Traxler MF, Chang DE, Conway T. Guanosine 3',5'-bispyrophosphate coordinates global gene expression during glucose-lactose diauxie in *Escherichia coli*. Proc Natl Acad Sci USA. 2006;103(7):2374–9. doi: 10.1073/pnas.0510995103.

59. Traxler MF, Summers SM, Nguyen HT, Zacharia VM, Hightower GA, Smith JT, et al. The global, ppGpp-mediated stringent response to amino acid starvation in *Escherichia coli*. Mol Microbiol. 2008;68(5):1128–48. doi: 10.1111/j.1365-2958.2008.06229.x.

60. Gaca AO, Colomer-Winter C, Lemos JA. Many means to a common end: the intricacies of (p)ppGpp metabolism and its control of bacterial homeostasis. J Bacteriol. 2015;197(7):1146–56. doi: 10.1128/JB.02577-14.

61. Liu K, Bittner AN, Wang JD. Diversity in (p)ppGpp metabolism and effectors. Curr Opin Microbiol. 2015;24:72–9. doi: 10.1016/j.mib.2015.01.012.

62. Kalisky T, Dekel E, Alon U. Cost-benefit theory and optimal design of gene regulation functions. Phys Biol. 2007 Nov;4(4):229–45. doi: 10.1088/1478-3975/4/4/001.

63. Poelwijk FJ, de Vos MGJ, Tans SJ. Tradeoffs and optimality in the evolution of gene regulation. Cell. 2011 Aug;146(3):462–70. 00023. doi: 10.1016/j.cell.2011.06.035.

64. Bakshi S, Siryaporn A, Goulian M, Weisshaar JC. Superresolution imaging of ribosomes and RNA polymerase in live *Escherichia coli* cells. Mol Microbiol. 2012;85(1):21–38. doi: 10.1111/j.1365-2958.2012.08081.x.

65. Gausing K. Regulation of ribosome synthesis in *E. coli*. In: Chambliss G, Craven GR, Davies J, Davis K, Kahan L, Nomura M, editors. Ribosomes: Structure, Function and Genetics. Baltimore: University Park Press; 1980. p. 693–718.

66. Zengel JM, Lindahl L. Transcription of ribosomal genes during a nutritional shift-up of *Escherichia coli*. J Bacteriol. 1986;167(3):1095–7.

67. Friesen JD, Fiil NP, von Meyenburg K. Synthesis and turnover of basal level guanosine tetraphosphate in *Escherichia coli*. J Biol Chem. 1975;250(1):304–9.

68. Young JW, Locke JC, Altinok A, Rosenfeld N, Bacarian T, Swain PS, et al. Measuring single-cell gene expression dynamics in bacteria using fluorescence time-lapse microscopy. Nat Protoc. 2011;7(1):80–8. doi: 10.1038/nprot.2011.432.

69. Duncombe TA, Tentori AM, Herr AE. Microfluidics: reframing biological enquiry. Nat Rev Mol Cell Biol. 2015;16(9):554–67. doi: 10.1038/nrm4041.

70. Molin S, Meyenburg KV, Maaloe O, Hansen MT, Pato ML. Control of ribosome synthesis in *Escherichia coli*: Analysis of an energy source shift-down. J Bacteriol. 1977;131(1):7–17.

71. Venayak N, Anesiadis N, Cluett WR, Mahadevan R. Engineering metabolism through dynamic control. Curr Opin Biotechnol. 2015;34:142–52. doi: 10.1016/j.copbio.2014.12.022.

72. Dahl RH, Zhang F, Alonso-Gutierrez J, Baidoo E, Batth TS, Redding-Johanson AM, et al. Engineering dynamic pathway regulation using stress-response promoters. Nat Biotechnol. 2013;31(11):1039–46. doi: 10.1038/nbt.2689.

73. Xu P, Li L, Zhang F, Stephanopoulos G, Koffas M. Improving fatty acids production by engineering dynamic pathway regulation and metabolic control. Proc Natl Acad Sci USA. 2014;111(31):11299–304. doi: 10.1073/pnas.1406401111.

74. Izard J, Gomez Balderas C, Ropers D, Lacour S, Song X, Yang Y, et al. A synthetic growth switch based on controlled expression of RNA polymerase. Mol Syst Biol. 2015;11(11):840. doi: 10.15252/msb.20156382.

75. Storn R, Price K. Differential evolution – a simple and efficient heuristic for global optimization over continuous spaces. J Glob Optim. 1997 Dec;11(4):341–59. doi: 10.1023/A:1008202821328.

76. Borisov VF. Fuller's phenomenon: Review. J Math Sci. 2000 Jul;100(4):2311–54. doi: 10.1007/s10958-000-0001-9.

77. Filippov AF. Differential Equations with Discontinuous Right-hand Sides. Dordrecht: Kluwer Academic Publishers; 1988. doi: 10.1007/978-94-015-7793-9.

78. Cohen SD, Hindmarsh AC. CVODE, a stiff/nonstiff ODE solver in C. Comput Phys. 1996;10(5):138–43. doi: 10.1063/1.4822377.

79. Hindmarsh AC, Brown PN, Grant KE, Lee SL, Serban R, Shumaker DE, et al. SUNDIALS: Suite of Nonlinear and Differential/Algebraic Equation Solvers. ACM Trans Math Softw. 2005;31(3):363–96. doi: 10.1145/1089014.1089020.

80. Uter NT, Perona JJ. Long-range intramolecular signaling in a tRNA synthetase complex revealed by pre-steady-state kinetics. Proc Natl Acad Sci USA. 2004 Oct;101(40):14396–401. doi: 10.1073/pnas.0404017101.

81. Freist W, Gauss DH, Ibba M, Söll D. Glutaminyl-tRNA synthetase. Biol Chem. 1997 Oct;378(10):1103–17.

82. Hachiya T, Terashima I, Noguchi K. Increase in respiratory cost at high growth temperature is attributed to high protein turnover cost in Petunia x hybrida petals. Plant Cell Environ. 2007 Oct;30(10):1269–83. doi: 10.1111/j.1365-3040.2007.01701.x.

83. Yamamoto T, Izumi S, Gekko K. Mass spectrometry of hydrogen/deuterium exchange in 70S ribosomal proteins from *E. coli*. FEBS Lett. 2006 Jun;580(15):3638–42. doi: 10.1016/j.febslet.2006.05.049.

84. Bennett BD, Kimball EH, Gao M, Osterhout R, Van Dien SJ, Rabinowitz JD. Absolute metabolite concentrations and implied enzyme active site occupancy in *Escherichia coli*. Nat Chem Biol. 2009 Aug;5(8):593–9. doi: 10.1038/nchembio.186.

85. Churchward G, Bremer H, Young R. Macromolecular composition of bacteria. J Theor Biol. 1982 Feb;94(3):651–70. doi: 10.1016/0022-5193(82)90305-8.

86. Zhou Y, Vazquez A, Wise A, Warita T, Warita K, Bar-Joseph Z, et al. Carbon catabolite repression correlates with the maintenance of near invariant molecular crowding in proliferating *E. coli* cells. BMC Syst Biol. 2013 Dec;7:138. doi: 10.1186/1752-0509-7-138.

87. Zimmerman SB, Trach SO. Estimation of macromolecule concentrations and excluded volume effects for the cytoplasm of *Escherichia coli*. J Mol Biol. 1991 Dec;222(3):599–620. doi: 10.1016/0022-2836(91)90499-V.

88. McGuffee SR, Elcock AH. Diffusion, crowding & protein stability in a dynamic molecular model of the bacterial cytoplasm. PLoS Comput Biol. 2010 Mar;6(3):e1000694. doi: 10.1371/journal.pcbi.1000694.

89. Marchal C. Chattering arcs and chattering controls. J Optim Theory Appl. 2013 Aug;11(5):441–68. doi: 10.1007/BF00935659.

90. Trélat E, Zuazua E. The turnpike property in finite-dimensional nonlinear optimal control. J Differ Equ. 2015 Jan;258(1):81–114. doi: 10.1016/j.jde.2014.09.005.